Master Thesis, Department of Geosciences

Dynamic simulations of landslide runout in cohesive soils

Tesfahunegn Abera Gebreslassie

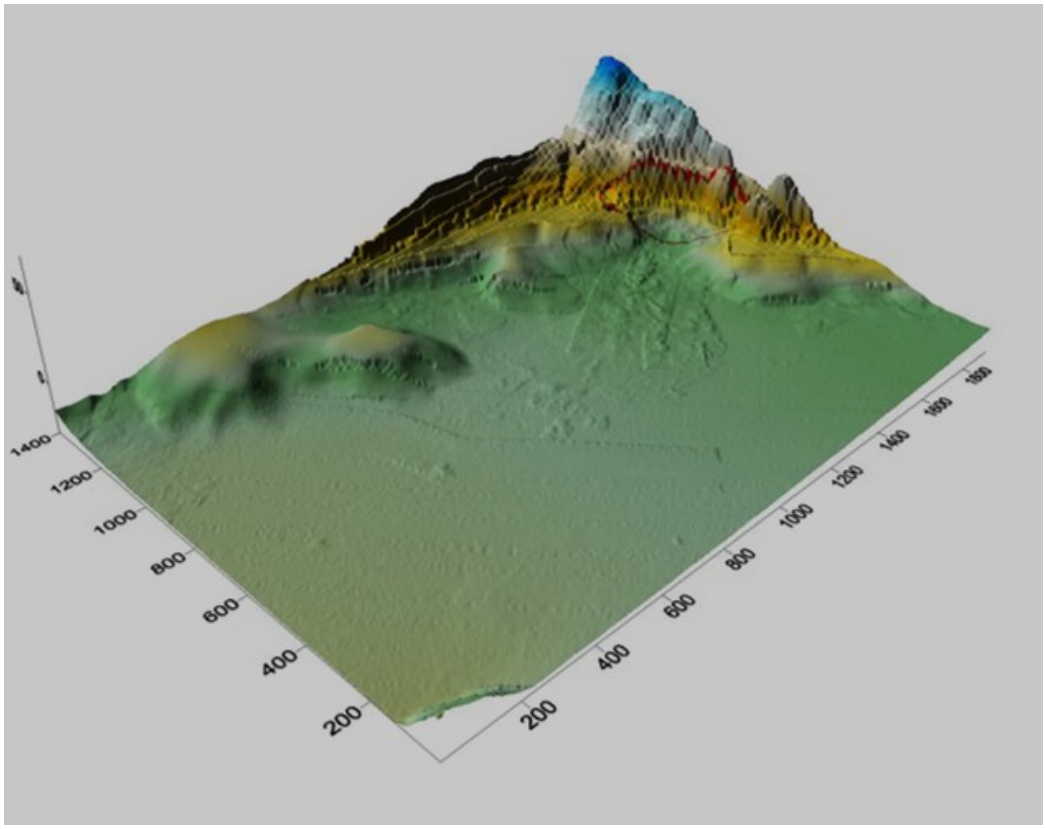

UNIVERSITY OF OSLO
FACULTY OF MATHEMATICS AND NATURAL SCIENCES

Dynamic simulations of landslide runout in cohesive soils

Tesfahunegn Abera Gebreslassie

Master Thesis in Geosciences

Discipline: Environmental Geology and Geohazards

Department of Geosciences

Faculty of Mathematics and Natural Sciences

University of Oslo

Spring, 2015

Tutors: 1. Farrokh Nadim (NGI) 2. José Cepeda (NGI) and 3. Karen Mair (UiO).

This work is published digitally through DUO – Digitale Utgivelser ved UiO

http://www.duo.uio.no

It is also catalogued in BIBSYS (http://www.bibsys.no/english)

Acknowledgements

First and foremost, Praise to the Almighty of God and His beloved Mother, for leading my life through the best chances one could imagine, regardless of who I am.

My special gratitude goes to the University of Oslo (UiO) and Norwegian Geotechnical Institute (NGI) for providing me data and space to conduct this research.

I would like to thank my supervisors Farrokh Nadim (Prof.), José Cepeda (PhD) and Karen Mair (Associate Prof.) for their guidance and supervision throughout the research time.

My special thanks goes to José Cepeda for his daily following up and his advices in data processing in ArcGIS, Surfer, BING model, DAN3D model and other softwares to achieve this work. I would also like to thank José for providing me the necessary input data (DEM) for the model.

I would like to express my special gratitude to the Norwegian State Educational Loan Fund (Lånekassen) for granting me the fund to study at the department of Geosciences under the program of Environmental Geology and Geohazards in the University of Oslo.

I would also like to thank all my teachers, classmates, friends and staff members of the Geosciences department and Norwegian Geotechnical Institute for wonderful time in Oslo, Norway.

Last but not least, I would like to express my special gratitude to my family for the encouragement and nice advice during this work.

Abstract

Recently, population and development approach closer to mountainous regions and other landslide prone areas. Since landslides produce loss of life and damaging to property, monitoring and analysing the runout behaviour of landslides using numerical models becomes crucial. In Scandinavian countries, quick-clay slides are among the most catastrophic events compared to other landslide types. Therefore, the main objective of this thesis is simulation of landslide runout in cohesive soils. A synthetic benchmarking and the Finneidfjord quick-clay slide were considered as case and were simulated using the DAN3D and BING models. The models are totally based on topography and material parameters.

Synthetic benchmarking simulation was done using both rheologies of the DAN3D and BING models. Runout distances and flow velocities were analysed and showed reasonable results. However, using DAN3D Bingham rheology the maximum runout extends beyond the domain of the simulation. In the BING simulation the end of the simulation time was very small compared to the DAN3D model. Runout distance is the longest in DAN3D model simulation using plastic rheology and maximum velocity is the highest in the BING simulation.

The Finneidfjord quick-clay landslide was simulated using both plastic and Bingham rheology in the DAN3D model for two different volume of initiation. The lower and higher volumes used were 945,000 & 1,220,000 m^3 respectively. This landslide was also simulated using the BING model. Runout distances and flow velocities were analysed for each cases.

Runout of the simulation was compared with plastic rheology for the first 200 seconds and it was found that runout in the case of Bingham was shorter. In general, the runout distance was longer for case of DAN3D model and the maximum velocity occurred in the case of the BING model.

Simulations using plastic rheology in the case of DAN3D and BING have shown reasonable results compared to the Bingham rheology using DAN3D.

Keywords: DAN3D, BING, plastic, Bingham, benchmarking, Finneidfjord, simulation.

List of abbreviations and notations

ASCII - American standard code for information interchange

DEM - Digital elevation model

GIS - Geographical information system

NGF - Norsk Geotekniske Forening (Norwegian Geotechnical Society)

NGI - Norwegian geotechnical institute

NVE - Norwegian Water Resources and Energy Directorate (Norges Vassdrags og Energidirektorat)

SPH - Smoothed particle hydrodynamics

UiO - University of Oslo

D = thickness of debris

D_p = thickness of plug flow layer

Ds = thickness of shear layer

n = Herschel-Bulkley exponent

$\alpha_1, \alpha_2, \beta =$ Constant shape factors

γ_r = Reference strain rate

γ = Yield strength

ρ_q = Quick clay density

ρ_w = Water density

Table of Contents

List of tables

List of figures

1. Introduction

1.1 General background

Now a day the population density and development of mountainous terrains bring human settlements within reach of landslide hazards (Pirulli, 2005). Because of this, it needs attention and assessment of hazard and risk management.

Landslides are geological hazards that commonly occur in mountainous areas in different part of the world. Landslides may produce loss of life and property. Among the different types of landslides, quick clay slides may evolve in catastrophic events in Scandinavian countries and Canada (Nigussie, 2013). They can travel at very high velocities and affect inhabited areas, transportation routes, farmland, and various types of infrastructures. Landslides involve the spontaneous failure of entire mountain slopes, involving volumes measured in tens or hundreds millions cubic meters and travel several kilometers (Pirulli, 2005). Risk evaluation of these events requires the understanding of two fundamental problems, the initiation and the runout. The latter consists on the flowing and stopping phase of the mass of the landslide which is considered in this work.

According to Issler et al., (2012), Landslides in sensitive clays fall in four main classes: single rotational slides, multiple retrogressive slides, translational progressive landslides and spreads. Detail additional explanation about the different classes can be found in Nigussie, (2013).

Runout is a key component in the hazard and risk assessment of high mobility landslides, such as those occurring in quick clay soils. Its assessment is useful both for hazard and risk mapping and the design of mitigation measures (Clague and Stead, 2012). Its analysis can be defined as the prediction of landslide dynamics and consequences. Currently, numerical models for simulating landslide runout are increasingly used for elaborating risk and hazard maps (Pastor and Luna, 2012).

The most important part of landslide hazard assessment revolves around the prediction of the failure and the runout of the landslide. The latter needs accurate prediction of the intensity of landslide. Runout can be characterized by the quantitative distribution of parameters like

travel distance, width, depth and velocity of the landslide mass, volume of the mass and others (Hungr, 1995). The present study will focus on the runout distance of landslides and their velocities. The runout behavior can be described by a set of spatially distributed quantitative parameters like area potentially affected by the slide, spatial distribution of the velocity, pressure, depth of the moving mass and depth of the deposits (Pastor and Luna, 2012).

Numerical models have become a fundamental tool to obtain approximations to engineering and science problems because many of them do not have analytical solution (Pastor and Luna, 2012). Numerical simulations provide a useful tools for investigating within the realistic geological contexts, the dynamics of the flows and of their arrest phase (Pirulli, 2005). In the 1970's the most widely used and perhaps earliest model proposed for the analysis of rockslides and similar phenomena was that of a rigid block on an inclined plane. In addition to this laboratory experiments were done in order to better understand the movement or runout behavior and motivated the introduction of more sophisticated apparatus (Pirulli, 2005). Presently, there are various methods of analysis of landslide runout. These include from simple empirical-statistical relationships to complex three-dimensional numerical modelling (Clague and Stead, 2012). This research will focus on the numerical types. In most of these numerical models, runout is a key element to analyze the behavior of a landslide quantitatively.

Once a landslide is released, the variation in the modes of movement and the different processes occurring while the flow is in movement influences the flow velocity and travel distance. Because of this situation, there is no universal runout model. It means that no single model can adequately describe all landslide types (Luna, 2012). Therefore, comparing and taking different numerical models to analyze the runout of landslides is crucial.

The advantage of numerical methods, is that they have the power for computing the movement of flow over irregular topographic terrain with a good compromise between computing effort and accuracy. The computed output of the model gives the intensity of the landslide and they provide the opportunity to investigate runout frequencies and magnitudes of landside in the absence of documented files (Pastor and Luna, 2012).

In this work, a numerical model of dynamic analysis called DAN3D will be used and this model can model post failure motion. In addition to DAN3D, the BING model will also be

applied for a case study and a synthetic benchmark. The case study is taken from previously occurred quick-clay slide located in the Finneidfjord area, Northern part of Norway.

Most of numerical models are based on computational grids. A new group of meshless numerical methods has been developed in the past decades (Pastor et al., 2009). One of these methods is called smoothed particle hydrodynamics, SPH. As it is mentioned in Pastor et al., (2009), SPH is a meshless numerical method introduced by different researchers and it was applied for the first time for astrophysical modelling. This model can be also applied propagation of landslides.

The governing equations of numerical models that described both DAN3D and BING simulations were presented below in section 2 below.

1.2 Statement of the problem and motivation of the study

Landslide runout is presently one of the most dangerous events among all geohazards types. Modelling runout of landslides helps to understand the behavior of landslides to design adequate protection measures and to assess evacuation times for the population. The important point of runout modeling is to predict accurate dynamics and the potential area that might be affected after a failure (Luna, 2012).

Numerical back analysis of Finneidfjord landslide, that is the case study considered in this work, was done using both the BING and DAN3D models. The DAN3D model had previously been applied to Finneidfjord landslide using a plastic rheology (Issler et al., 2012). It was also simulated with coarser resolution DEM for the submarine part of the terrain.

The motivation of the study is the availability of the new version of the model, DAN3D with Bingham rheology already implemented (previously only the plastic rheology was possible for cohesive landslides), availability of a higher resolution DEM of the study area, and to continue/extend the analysis from the previous study performed by Issler et al., (2012). Therefore, this study intendes to investigate the model with implementation of Bingham rheology and compare the results between the two models for both case studies. The two cases which will be simulated using DAN3D and BING are Finneidfjord landslide and synthetic benchmark.

1.3 The main objective of the study

The main objective of the research is dynamic simulation of landslide runout in cohesive soils considering both the Finneidfjord landslide and a synthetic benchmarking using DAN3D of new version of the model with the Bingham rheology, and the model BING. This will allow improving the understanding of the behavior of these landslides and updating the previous assessment (Issler et al., 2012). In addition to these, this work helps to better understand the model and its application to failure of landslides.

1.4 Procedure of simulation of the models

Both Surfer and ArcGIS software were used to process the DEM of the study sites as input to run the model (DAN3D). A 5 m cell DEM was used for the simulation through mosaicking the land and fjord part of the study site for the Finneidfjord landslide which were made available from NGI (Issler et al., 2012). Before running the model, two DEMs have to be prepared a path topography file and a source depth topography file. Path topography file is defined as the topography of the sliding surface over which the slide flows, and source topography file is defined as the vertical depth topography of the sliding mass at initial time position (Hungr, 2010). Simulation was done as indicated in the flow chart presented in Figure 1. This flow chart shows the procedure on how to run DAN3D model. The BING model was also run using the same rheological parameters as DAN3D and the flow chart is shown in Figure 2.

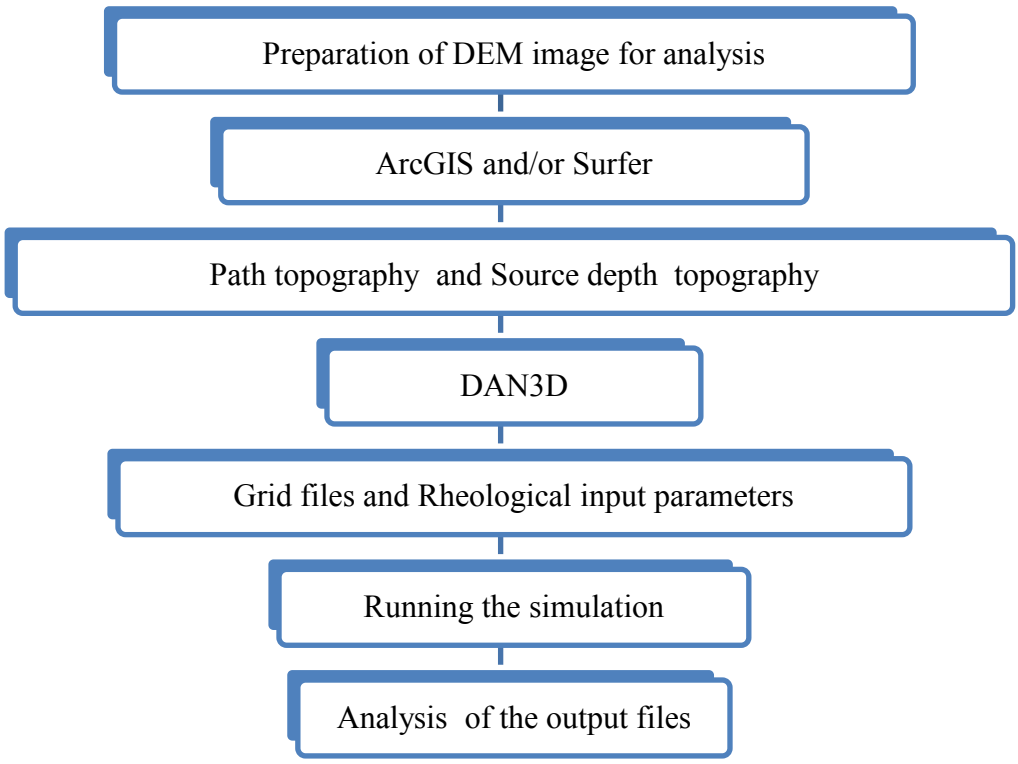

Figure 1: Procedure and flow chart for the DAN3D model simulations.

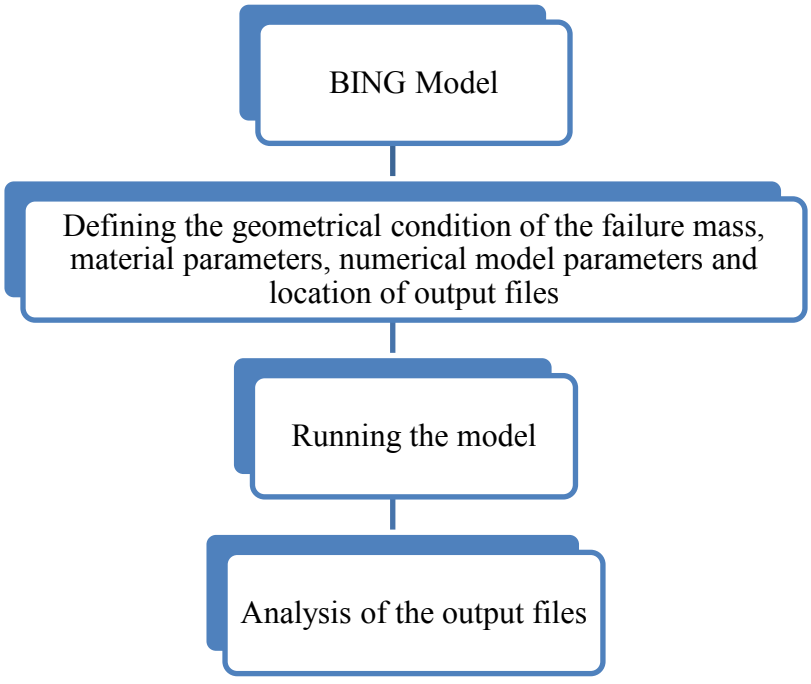

Figure 2: Procedure and flow chart for BING model.

1.5 Description of the study area

Norway is one of the Scandinavian countries, which have quick-clay soils. The most common quick-clay slides so far occurred in Norway include Rissa landslide, Finneidfjord landslide and Byneset slides. Finneidfjord landslide has considered in the simulation of the models. Besides to Finneidfjord landslide, synthetic benchmarking was also taken into consideration in the simulation of the models.

1.5.1 Finneidfjord landslide, Hemnes Municipality, Nordland county

Finneidfjord landslide is located in northern part of Norway. This landslide occurred in June 20, 1996 with a volume of 1 million m^3 sediments and with causality of four people. It is a kind of retrogressive flow of quick-clay slide that was happened along the shore line (Nigussie, 2013). As it was explained in Nigussie, (2013), this slide has been triggered because of excess pore pressure development after high precipitation. The failure of slide occurred in three main stages (initial slide, the main slide and minor slides along the slide scarp) (Longva et al., 2003). Location map of Finneidfjord landslide and release area of the slide are shown in Figure 3. This map shows the actual case of the landslide in the Finneidfjord area and it helps to compare simulation results of the model.

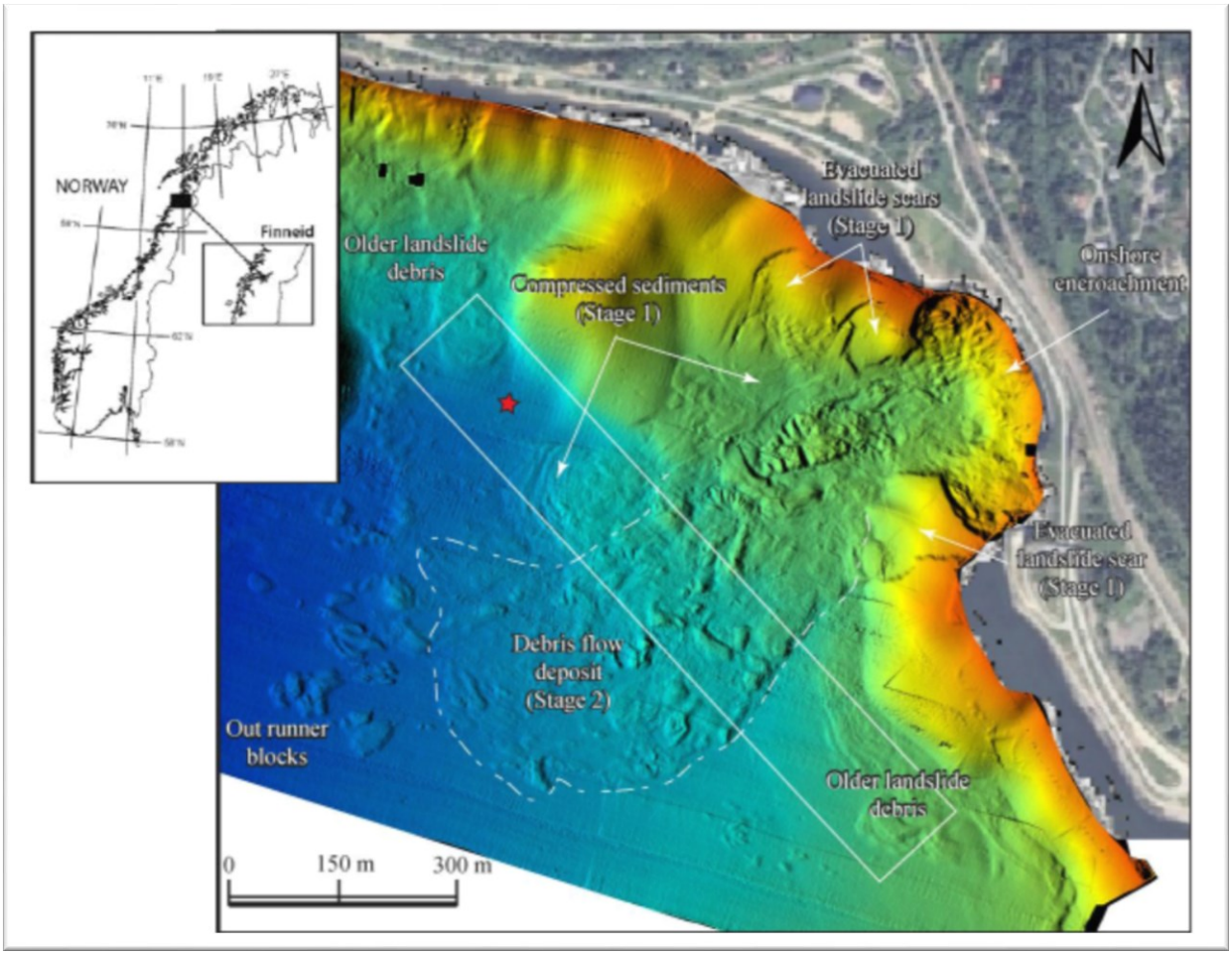

Figure 3: Geographic location of Finneidfjord and surface morphology of the 1996 slide from high resolution swath bathymetry with the different stages of the slide (Longva et al., 2003), (Issler et al., 2012) and (Woldeselassie, 2012).

1.6 Characteristics of quick clays

According to L'Heureux, (2012), in Norway the classification of clay material as quick is based upon the sensitivity (S_t) of the soil-the ratio between the undrained shear strength S_u and the remoulded shear strength S_{ur} and a threshold value of the remoulded shear strength. Clays are classified as quick when the remoulded shear strength is less than 0.5kPa and the sensitivity is greater than 30 (NGF, 1974). The recent guideline according to the Norwegian water and energy directorate (NVE), recommending the use of sensitivity (S_t) $\geq$ 15 and remoulded shear strength (S_{ur}) $\leq$ 2kPa for brittle clay material which collapse during a landslide (NVE, 2009).

1.6.1 Formation and origin of quick-clays

Most of the marine clay deposits are accumulated in the sea and fjords as a result of the last ice age glaciation and this lead to the sensitive clays soils (Nigussie, 2013). Leaching of ions has taken place for long time since the permeability of clay material is low (L'Heureux, 2012). Leaching by fresh groundwater results in the high sensitivity of these clays. The high sensitivity of Norwegian quick-clays is attributed to the leaching of ions (L'Heureux, 2012). Fresh groundwater percolating downwards through the marine deposits due to surface runoff or upwards due to artesian pressures removes the salt ions and leaves behind the unstable sensitive clay material with flocculated structure (Nigussie, 2013). Upon remoulding, this unstable structure is destroyed and the inter-particle surface water that is liberated gives rise to a liquid type fluid. This potential to liquefy when subjected to loading is one of the main agents governing the post-failure behaviour of quick-clays. The marine deposit of quick-clay is shown in Figure 4 and it is taken from (Løken, 1983).

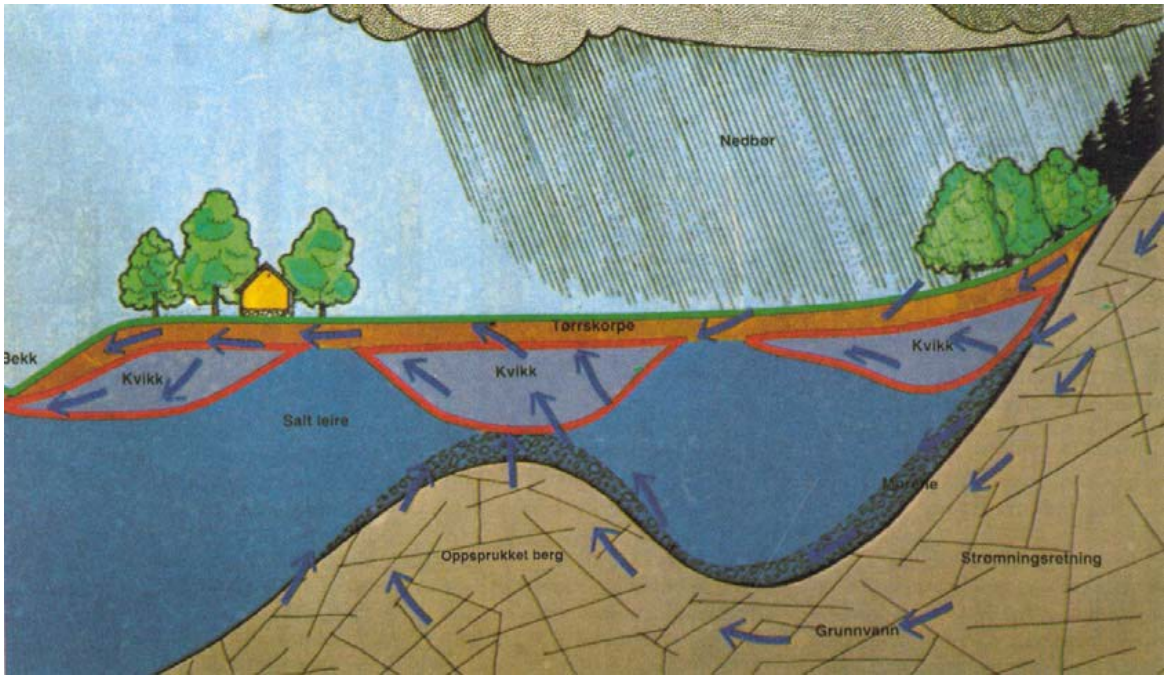

Figure 4: Conceptual model that show where quick-clays are found (Løken, 1983)

1.6.2 Geometrical representation of quick-clay slides

Geometrical representation of landslides is crucial to characterize and study in detail. Figure 5 is well documented geometrical representation of quick-clay slide taken from Natterøy, (2011) as it was mentioned in Nigussie, (2013).

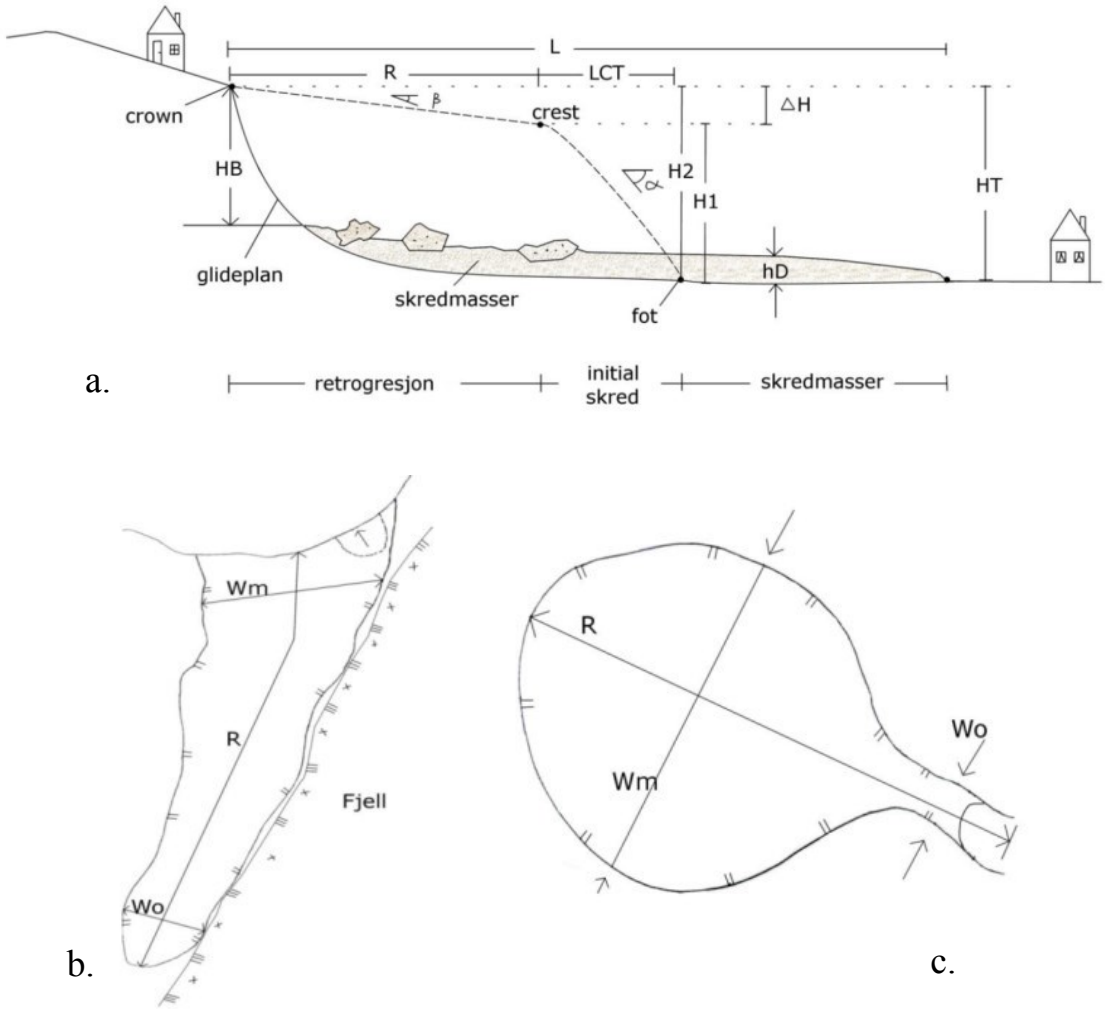

Figure 5: Geometrical representation of quick-clay slides. a) Cross section b) and c) Top view. Glide plane also called rupture surface where the slide mass (skredmasser) moves along. h_D – deposit depth, H_T – total drop height, H_1 – initial drop height, H_2 – vertical extent of failed volume, ΔH – altitude difference along back slope, H_B – escarpment height, L – total run out length, L_{CT} – length of fore slope, R – retrogression distance, W_0 – minimum width of the release gate, W_m – maximum width of the release area (Natterøy, 2011).

1.6.3 Types of landslides in quick-clay

Generally, there are four main types of landslides that can be observed in the quick-clays. These include single rotational slides, multiple retrogressive slides (earthflows or flows), translational progressive landslides and spreads. Among the large landslides occurring in quick-clays, flow types are the most common in Norway. The different type of landslides that occur in quick-clays can be seen in Figure 6 and it is taken from L'Heureux, (2012). The different types of landslide that occurred in quick clay in the country (Norway) are presented in the appendix 2 that was adapted from L'Heureux, (2012). Besides, to the type of landslides, their geotechnical parameters are also presented in appendix 3.

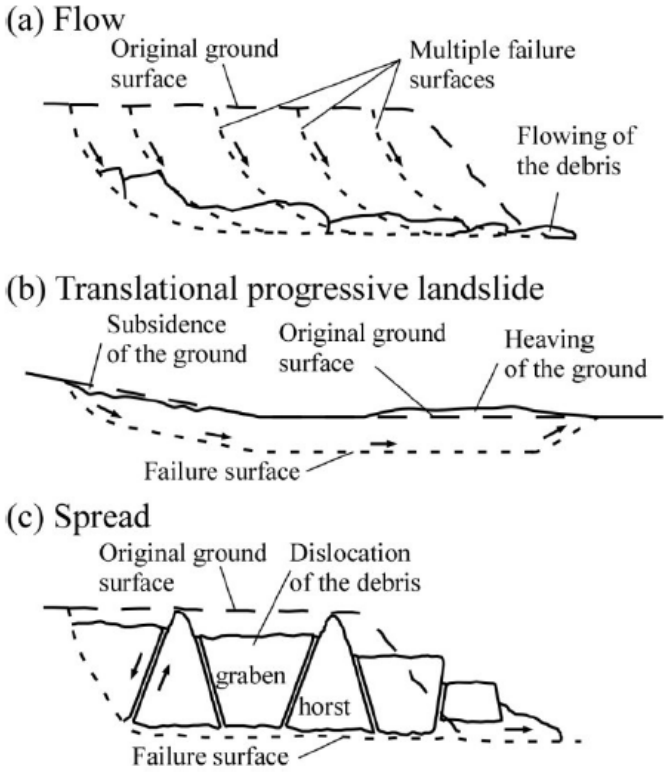

Figure 6: Types of landslide in quick-clay: a) multiple retrogressive landslide or flow, b) translational progressive landslide or flake, and c) spread (L'Heureux, 2012).

1.7 Outline of the thesis

This work has about five main chapters and the detail will follow in a separate sections.

Chapter 1: **Introduction** – in this part it is introduced the general background of landslides and their consequences. Besides, to these, it has introduced the different types of models and finally focused to the models used in this work. It has explained basic concepts about the models used in this work, statement of problem, objective, description and location map of Finneidfjord slide and characteristics of quick clays. Geometrical representation of quick clay and types of landslide in quick clay were also included in this section.

Chapter 2: **Mathematical description and expression of the models** - in this part it has defined the models, the governing equations, the two frameworks (Eulerian and Lagrangian) and parameterizing of the models. Mathematical explanation of BING model was also included in this chapter, which is crucial to understand the mathematical explanation behind the model. This part helps to understand the behaviour of simulation and characteristics of the models.

Chapter 3: **Simulation result of the models** – this part is presented the main result of the models for the case study considered in the thesis. Simulation result of both rheologies (plastic and Bingham) using the different volume slides were presented. Besides to these, synthetic DEM for benchmarking was applied to understand the simulation of the model. BING model was run to compare the results with DAN3D model simulations.

Chapter 4: **Discussion of simulation results of the models** - it is included the discussion part of the different result of the models. Simulation results were discussed for the different rheologies with graphs and maps. Comparison was also made between the two rheologies that were considered in this work for DAN3D model. Comparison between the two models were discussed and analysed. The analysed results were compared with the actual landslide.

Chapter 5: **Conclusions and recommendations for future work** - the conclusions reached by this work is presented in this part and forwarded some recommendations to be considered for further investigation. That is all that is conducted in this research work.

2. Mathematical description and explanation of the models

Numerical methods for modeling runout behavior of landslides mainly include fluid mechanical models and distinct element methods. The most common and used approach for this method is based on continuum mechanics. Continuum fluid mechanics models utilize the conservation equations of mass, momentum and energy that explain the dynamic motion of the landslides (Luna, 2012).

2.1 BING model

According to the NGI report written by Issler et al., (2012), Bingham is a quasi-two dimensional numerical model of the downslope spreading of a finite source subaqueous debris flow that incorporates the Bingham, Herschel-Bulkley (H-B), and bilinear rheologies for visco-plastic fluids. It is a user defined alternatively based on the available data, the type and source of material involved. The short form of Bingham is BING and it is used with this name in most models (Imran et al., 2001a).

The shape of mass failure in this case is assumed to be parabolic and this is completely described by the position of tail, the length and maximum height of the failure material (Imran et al., 2001a).

The governing equations describing the conservation of mass and momentum of a landslide flow on an arbitrary topography are transformed into a Lagragian framework and solved using an explicit time marching finite difference scheme. The Lagragian equations can be solved with the help of a deformable grid system that moves together with the flow of mass (Imran et al., 2001a). These different equations are presented below.

The slender flow approximation used in the analysis retains only one component of shear stress, i.e. the component τ_{xy}, where x denotes a boundary-attached downslope coordinate and y denotes a coordinate upward normal from the bed. Here τ_{xy} is abbreviated to τ. The Herschel-Bulkley rheology is obtained from the relation

$$\frac{\gamma}{\gamma_r} = \begin{cases} 0 & for\ \tau \leq \tau_y \\ \left(\frac{\tau}{\tau_y} - 1\right)^{1/n} & for\ \tau > \tau_y \end{cases} \quad (1)$$

where τ_y denotes a yield strength, n is an exponent and $\gamma = \frac{\partial u}{\partial y}$ denotes the xy component of the local strain rate and γ_r denotes a reference strain rate. For the case $\tau > \tau_y$, the rheology reduces to the more familiar form

$$\tau = \tau_y + K\gamma^n \tag{2}$$

where $K = \frac{\tau_y}{\gamma_r^n}$

The limiting case $n = 1$ yields the Bingham rheology, for which K becomes synonymous with the dynamic viscosity μ_d of the debris slurry and it is given in the following equation (De-Blasio, 2011):

$$\tau = \tau_y + u_d\gamma$$

BING obtains the extra information required for determining the plug-layer depth by solving not one, but two momentum balance equations – one integrated over the entire flow depth and the other one integrated only over the plug layer (Issler et al., 2012).

In Herschel-Bulkley fluids, there is a region called plug layer, where there is no shear because the shear stress is below the yield strength. In a flow mass the plug layer extends from the upper surface some depth into the flow mass; next to that is the shear layer. The schematic representation is indicated in Figure 7. The plug layer an influence with slope angle, inertial forces due to acceleration or deceleration of the flow.

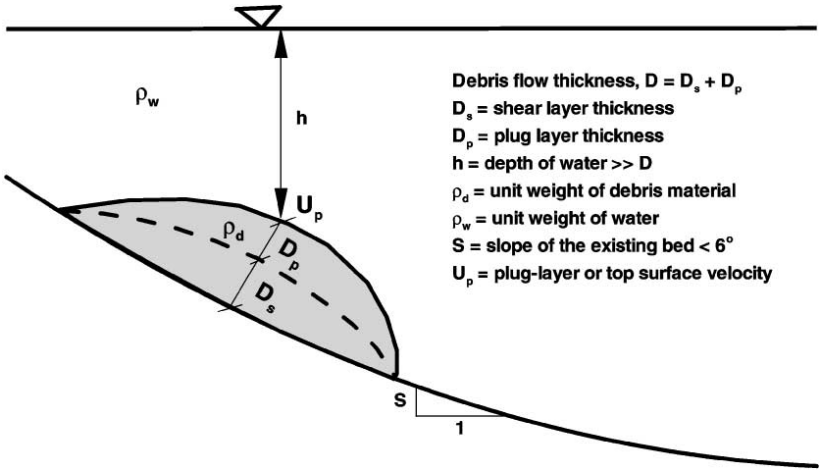

Figure 7: Schematic representation of mudflow (underwater) (Imran et al., 2001a) and (Issler et al., 2012).

For the Herschel-Bulkley formulation the analysis yields one equation of mass conservation and two of momentum conservation, one for a plug layer and the other for a shear layer immediately below. These relations are as follows;

$$\frac{\partial D}{\partial t} + \frac{\partial}{\partial x}\left[U_t\left(D_p + \alpha_1 D_s\right)\right] = 0$$

$$\frac{\partial}{\partial t}\left(U_t D_p\right) + U_t\frac{\partial D_s}{\partial t} + \frac{\partial}{\partial x}\left(U_t^2 D_p\right) + \alpha_1 U_t\frac{\partial}{\partial x}\left(U_t D_s\right) = -\left(1 - \frac{\rho_w}{\rho_d}\right) g D_p \frac{\partial D}{\partial x} + \left(1 - \frac{\rho_w}{\rho_d}\right) g D_p S - \frac{\tau_y}{\rho_d}$$

$$\alpha_1\frac{\partial}{\partial t}\left(U_t D_s\right) - U_t\frac{\partial D_s}{\partial t} + \alpha_2\frac{\partial}{\partial x}\left(U_t^2 D_p\right) - \alpha_1 U_t\frac{\partial}{\partial x}\left(U_t D_s\right) = -\left(1 - \frac{\rho_w}{\rho_d}\right) g D_s \frac{\partial D}{\partial x} + \left(1 - \frac{\rho_w}{\rho_d}\right) g D_s S - \beta\frac{\tau_y}{\rho_d}\frac{U_t}{\gamma_r D_s} \quad (3)$$

In the above relations g denotes the acceleration of gravity, ρ_w denotes the density of the ambient fluid, ρ_d denotes the density of the debris slurry, U_t denotes the stream wise velocity of the plug layer, D_p denotes the thickness of the plug layer, D_s denotes the thickness of the shearing layer below and D is the sum of D_p and D_s (as indicated in Figure 7). The parameters α_1, α_2 and β are constant functions of the exponent n that corresponds to the shape factor as outlined in (Imran et al., 2001a).

In the bilinear model there is no yield strength, so that the strain rate γ vanishes only when $\tau = 0$. It encompasses two limiting flow regimes however; at high strain rates the flow deforms with a relatively low viscosity and at low strain rates it deforms with a relatively high viscosity. The "apparent" yield strength associated with high strain rate is denoted as τ_{ya}. The rheology is described by the relation:

$$\tau = \tau_{ya}\left(1 + \frac{\gamma}{\gamma_r} - \frac{1}{1 + r\frac{\gamma}{\gamma_r}}\right) \quad (4)$$

where $r = \frac{\gamma_r}{\gamma_0}$ and $\gamma_r = \frac{\tau_{ya}}{\mu_h}$

In the above $\gamma_r >> \gamma_o$ are rheological constants with the dimensions of strain rate providing information about behavior at high and low strain rates, respectively. For example, when

$\gamma/\gamma_r >> 1$ the following Bingham relation with viscosity μ_{dh} is obtained at high shear stresses;

$$\tau \cong \tau_{ya} + \mu_{dh}\gamma \quad where\ \mu_{dh} = \frac{\tau_{ya}}{\gamma_r}$$

When $\gamma/\gamma_r << 1$ the following Newtonian relation with viscosity μ_{dl} is obtained at low shear stresses;

$$\tau \cong \mu_{dl}\gamma \quad where\ \mu_{dl} = \frac{\tau_{ya}}{\gamma_r}\ (1 + r)$$

Note that of necessity $\mu_{dl} >> \mu_{dh}$.

Since the bilinear formulation contains no yield strength, the integral analysis yields one equation for mass conservation and one relation for momentum conservation;

$$\frac{\partial D}{\partial t} + \alpha_1 \frac{\partial}{\partial x}(U_t D) = 0$$

$$\alpha_1 \frac{\partial}{\partial t}(U_t D) + \alpha_2 \frac{\partial}{\partial x}(U_t^2 D) = -\left(1 - \frac{\rho_w}{\rho_d}\right) gD \frac{\partial D}{\partial x} + \left(1 - \frac{\rho_w}{\rho_d}\right) gDS - \frac{\tau_y}{\rho_d}\varphi \qquad (5)$$

Here U_t denotes the stream wise velocity attained at the top of the flowing slurry. In addition α_1, α_2 and φ are constant functions of the dimensionless parameters $U_t/(\gamma_r D)$ and r, as specified in Imran et al., (2001a) and Jiang and LeBlond, (1993).

Input and output of BING model

The software provides a simple interface. Upon running BING model, an input window appears. This input window is divided into four sections (Figure 8); initial conditions, material parameters, numerical model parameters and output files (Imran et al., 2001b).

The output produced by BING includes the time variation of downstream front velocity as well as the spatial variation of flow thickness (height above the bed) as a function of time. The program also generates a graphical display of the spatial variation of flow thickness at various times during a run. This graph allows for monitoring of the general flow behavior and aids in the detection of numerical instabilities (Issler et al., 2012).

Output Display - graphical version shows the profile of the flow and gives the elapsed time, location of the head and head velocity; numeric version only shows the elapsed time, location of the head and head velocity (Figure 8). The rheological inputs that were considered to run BING model were taken from the physical parameters of Finneidfjord landslide case as shown in Table 1.

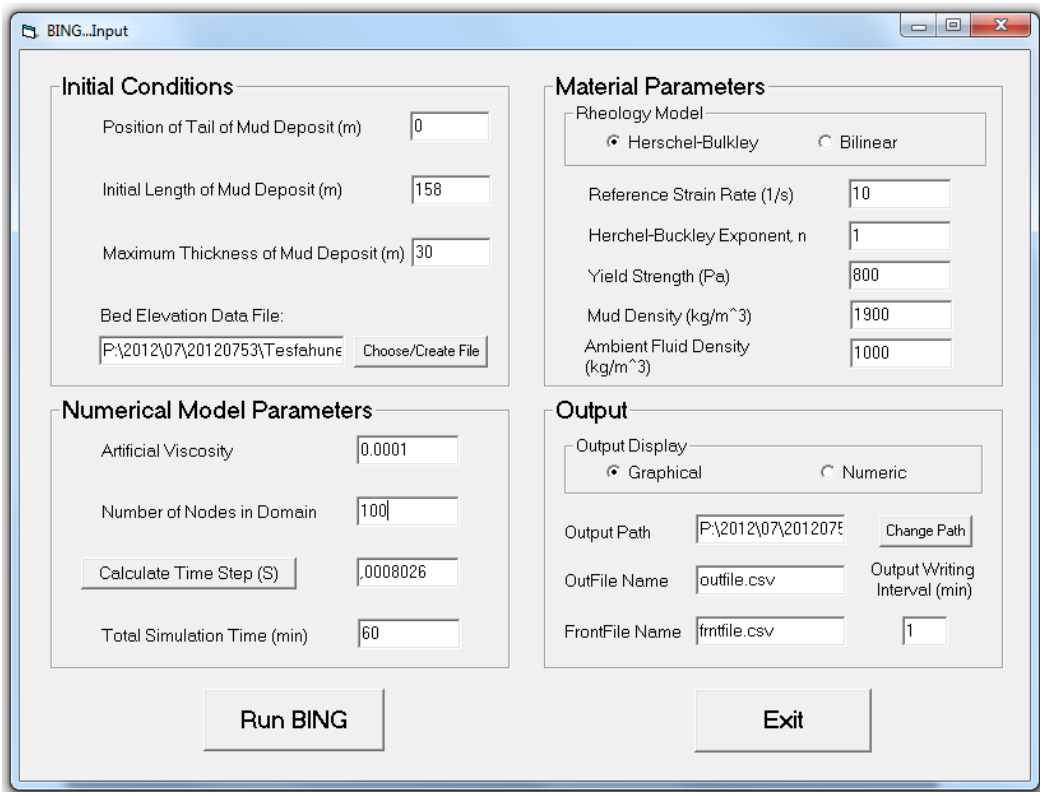

Figure 8: The input and output window of BING model and input parameters that are displayed corresponds to one of the run using the BING model.

2.2 DAN3D model

DAN3D (Dynamic Analysis of Landslides in Three Dimensions) is windows-based program that implement the numerical model for dynamic analysis of rapid flow slides, debris flows and avalanches (Luna, 2008). It is a tool suitable for estimating runout behaviour of landslides on the basis of specific data on geometry and material properties supplied by the user (Hungr, 2010).

Meshless Lagrangian frame work is adapted to run the simulation with Smoothed Particle Hydrodynamics (SPH, more about this is explained by Monaghan, (1992)): “Particles” endowed with properties corresponding to the dynamical variables move according to the

equations of motion, similar to cells in conventional Lagrangian schemes. However, the field values (flow height and momentum) at a given point are not determined by the cell in which this point presently is located, but calculated as a sum of contributions from all nearby "particles", weighted by a function of the distance between the particles and the point in question Figure 9. The weight function or "kernel" plays a central role in the mathematical formulation of this scheme; both its shape and spatial range can be chosen freely within certain limits.

The SPH method has been successfully applied to problems that are difficult to handle with mesh techniques, e.g., the breaking of waves, the impact of droplets onto a fluid or a solid wall and other situations where the flowing material splits. If the flow dilutes very strongly in certain regions, it may be necessary to redistribute the quantities of mass and momentum carried by a single isolated "particle" over several particles newly seeded around the original one (Issler et al., 2012).

Flow depth at reference column *i* can be calculated using the summation interpolant as it was mentioned in Luna, (2008) by Wang and Shen, 1999:

$$h_i = \sum_{j=1}^{N} V_j W_{ij}$$

Where W_{ij} is an interpolating karnel (weighting factor for proximity) and V_j is the volume of particle j. Figure 9 gives an example of this procedure.

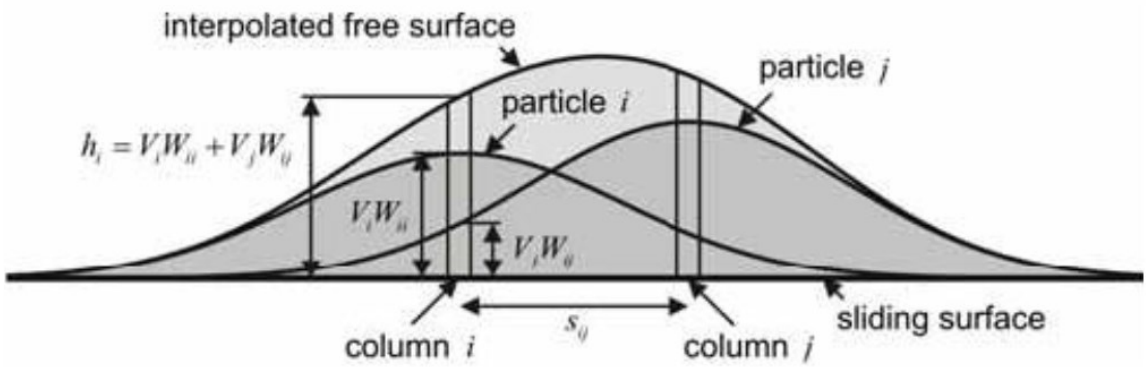

Figure 9: Schematic representation of the way SPH reconstructs flow height from the weighted contributions of all particles within a finite distance (Issler et al., 2012).

DAN3D model allows for the different resistant acting on the base of an internally frictional flow and the user can choose amongst the five rheological types available in the model.

These include; frictional, plastic, Newtonian, Bingham, and Voellmy (Hungr and McDougall, 2009). The equations for different resistance flow are derived from uniform flow equations corresponding to each given rheology, solving for the basal shear stress as a function of normal flow depth, density, mean flow velocity and rheological parameters (Nigussie, 2013).

The basal shear stress τ, opposes motion and due to the chosen reference coordinate system orientation is always negative. The mathematical expression and explanation of the bed shear stress are the following:

1. Frictional basal resistance: is given by the difference between normal stress and pore pressure at the bed. It is often exhibited by granular materials.

$$\tau = -(\sigma_z - u)\tan\emptyset \tag{6}$$

Where: $\emptyset$ is the dynamic basal friction angle, u is the pore pressure and σ_z is stress normal to the bed.

2. Voellmy resistance: is a combination of turbulent and frictional behavior. It is given by:

$$\tau = -\left(\sigma_z f + \frac{\rho g v^2}{\xi} V\right) \tag{7}$$

Where: f is the friction coefficient and ξ is turbulence parameter.

3. Newtonian flow: is the function of the velocity and viscosity parameter. It is given by:

$$\tau = \frac{3v\mu}{H} \tag{8}$$

Where: μ is the viscosity and v is the velocity of the sliding mass.

4. Bingham resistance: is a combination of plastic and viscous behaviour. A Bingham fluid is assumed to be viscous above a threshold yield stress and rigid below a threshold value. The basal resistance term is given by:

$$\tau^3 + 3\left(\frac{\tau_{yield}}{2} + \frac{\mu_{Bingham}}{2} V\right)\tau^2 - \frac{\tau_{yield}}{2} = 0 \tag{9}$$

Where: τ_{yield} is Bingham yield stress, $\mu_{Bingham}$ is the Bingham viscosity, V is the velocity and τ is basal shear resistance.

5. Plastic flow: is related with pseudo-static motion of liquefied soil, the base shear resistance is assumed to be equivalent to a constant yield strength value.

$$\tau = -c \tag{10}$$

Where: τ is the shear resistance along the bed.

Out of the five different rheologies explained above plastic and Bingham rheology are theoretically suitable for geotechnical analysis (Nigussie, 2013) and both of them were used in the simulation of the model. Selection of the rheology was based on the nature and behaviour of the slide and that was considered in the simulation of this case study.

DAN3D is capable of taking into account entrainment of eroded bed material into the flow (McDougall and Hungr, 2005). This is an important process in debris flows and snow avalanches, but appears to play a less prominent role in quick-clay slides. Because of this entrainment was not considered in this simulation. Besides to this, if you use only one material, entrainment is not important (Hungr, 2010).

2.3 Governing equations for DAN3D

The model is based on Lagrangian forms of depth integrated equations which is similar to the SPH. The governing equations begin from mass and momentum conservation laws governing the mechanics of a continuum (Hungr and McDougall, 2009):

$$\frac{\partial \rho}{\partial t} + \nabla \cdot \rho v = 0 \tag{11}$$

$$\frac{\partial(\rho \mathrm{v})}{\partial \mathrm{t}} + \nabla \cdot \rho \mathrm{v} \otimes \mathrm{v} = -\nabla \mathrm{T} + \rho \mathrm{g} \tag{12}$$

Where ρ material bulk density, t time v velocity vector T tress tensor g gravitational acceleration vector ∇ gradient operator $\cdot$ dot product and $\otimes$ tensor product.

By considering the material density is spatially and temporally constant, the two equations above become simplify to:

$$\nabla \cdot v = 0 \tag{13}$$

$$\rho\left(\frac{\partial v}{\partial t} + \nabla \cdot v \otimes v\right) = -\nabla T + \rho g \tag{14}$$

The total stress state on an element of material in an arbitrarily oriented, right-handed Cartesian coordinate system (*x, y, z*) is shown in Figure 10.

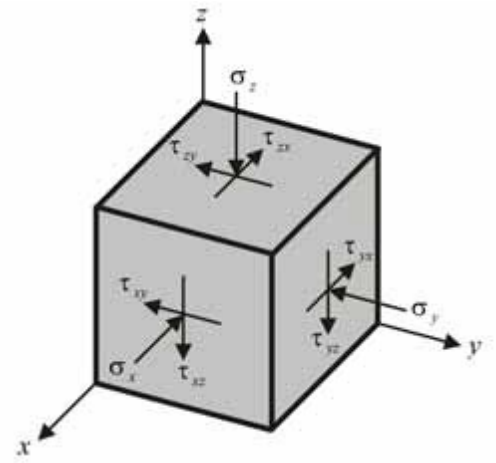

Figure 10: Total stress state on an element of material within a landslide. The stresses are considered positive as indicated. If z is aligned with the bed-normal direction, then τ_{zx} and τ_{zy} are the basal shear stresses for an element near the base of the flow (McDougall, 2006).

The stress tensor related to this material in Figure 10 can be described as in equation (15) below:

$$\boldsymbol{T} = \begin{bmatrix} \sigma_x & \tau_{xy} & \tau_{xz} \\ \tau_{yx} & \sigma_y & \tau_{yz} \\ \tau_{zx} & \tau_{zy} & \sigma_z \end{bmatrix} \tag{15}$$

Where: σ is total normal, and τ is total shear stresses.

Expanding equations (13) and (14) give the following system of mass and *x*, *y* and *z* direction momentum balance equations, respectively:

$$\frac{\partial v_x}{\partial x} + \frac{\partial v_y}{\partial y} + \frac{\partial v_z}{\partial z} = 0 \tag{16}$$

$$\rho\left(\frac{\partial v_x}{\partial t}+\frac{\partial(v_x^2)}{\partial x}+\frac{\partial(v_x v_y)}{\partial y}+\frac{\partial(v_x v_z)}{\partial z}\right)=-\left(\frac{\partial \sigma_x}{\partial x}+\frac{\partial \tau_{yx}}{\partial y}+\frac{\partial \tau_{zx}}{\partial z}\right)+\rho g_x \quad (17)$$

$$\rho\left(\frac{\partial v_y}{\partial t}+\frac{\partial(v_y v_x)}{\partial x}+\frac{\partial(v_y^2)}{\partial y}+\frac{\partial(v_y v_z)}{\partial z}\right)=-\left(\frac{\partial \tau_{xy}}{\partial x}+\frac{\partial \sigma_y}{\partial y}+\frac{\partial \tau_{zy}}{\partial z}\right)+\rho g_y \quad (18)$$

$$\rho\left(\frac{\partial v_z}{\partial t}+\frac{\partial(v_z v_x)}{\partial x}+\frac{\partial(v_z v_y)}{\partial y}+\frac{\partial(v_z^2)}{\partial z}\right)=-\left(\frac{\partial \tau_{xz}}{\partial x}+\frac{\partial \tau_{yz}}{\partial y}+\frac{\partial \sigma_z}{\partial z}\right)+\rho g_z \quad (19)$$

Equations (16) to (19) are the most general form of the incompressible continuum mass and momentum balance equations. Further simplified and integrated explanation about these equations can be found in (McDougall, 2006).

2.4 Eulerian versus Lagrangian

In dynamic modeling these two references are formulated. Eulerian reference frame is fixed in space and an observer standing still as a landslide passes. Models formulated in this frame work need solution of more complex form of the governing equations. This approach is a conventional method in computational fluid dynamics (McDougall, 2006). In contrary, Lagrangian reference frame moves with the local velocity and an observer riding on top of the landslide. This method simplifies the governing equations (McDougall, 2006).

The main problem here is the need of a very fine computational mesh for both the terrain information and for the fluidized soil. Lagrangian methods allow the separation of both meshes, with an important economy of computational effort. If we combine a Lagrangian method with a mesh based discretization technique, we will find problems as soon as the mesh deforms, making necessary to use mesh refinement. As alternative, meshless methods, which do not rely on meshes, avoids distortion problems in an elegant way. This is called smoothed particle hydrodynamics (SPH). It is a meshless method and it is applied firstly for astrophysical modelling (Blanc et al., 2011).

The SPH method is based on the equality. The different mathematical expression and integration for SPH method is as follow and it is adapted from Issler et al., (2012):

$$\phi(x) = \int_{\Omega} \phi\,(x')\delta(x' - x)dx' \tag{20}$$

where $\delta(x)$ is the Dirac delta. Traditionally, the Dirac delta 'function' is defined as

$$\delta(x) = \begin{cases} \infty, x = 0 \\ 0, |x| > 0 \end{cases} \tag{21}$$

With the additional requirement of 'unity'

$$\int_{\Omega} \phi\, \delta(x)dx = 1$$

Distributions are a class of linear functional and applications that transform functions into real numbers. They can be defined as

$$T_w[\phi] = \int_{\Omega} w\,(x')\phi(x')dx'$$

Where: $w(x')$ is referred to as the kernel of the linear functional, $T_w[\phi]$and $\phi(x')$ is called a test function.

Consider the sequence $w_k(x, h)$ of kernels

$$w_k(x, h) = \frac{1}{\sqrt{2\pi h}} \exp\left(-\frac{x^2}{h^2}\right), \text{where } h = 1/k \tag{22}$$

Where: the kernels depend on a length *h* or an integer *k*. dirac distribution in a weak sense as

$$\lim_{k\to\infty} T_{w\,k}\,[\phi] = \delta[\phi]$$

and

$$\lim_{h\to 0} \int_{\Omega} W_k\,(x' - x, h)\phi(x')dx' = \int_{\Omega} \phi\,(x')\delta(x' - x)dx' = \phi(x) \tag{23}$$

This expression can be immediately generalized to 2D or 3D, by considering a scalar or vector valued function $\phi(x)$ of $x\,\epsilon\,\Omega\,\mathbb{C}\,\mathbb{R}^{\mathrm{ndim}}$, where Ω is an open bounded domain.

Finally, these results are the starting point for constructing SPH approximations, where regular distribution are used to approximate the value of a function. The approximation is expressed as

$$\langle \phi(x) \rangle = \int_{\Omega} \phi\,(x') W(x' - x, h) dx' \tag{24}$$

The accuracy of SPH approximations depends on the properties of the kernel *W(x, h)*. A special class of kernels is that of functions having radial symmetry, i.e. depending only on *r*:

$$r = |x' - x| \tag{25}$$

It is convenient to introduce the notation

$$\xi = \frac{|x' - x|}{h} = \frac{r}{h} \tag{26}$$

because it allows one to express $W(x' - x, h)$ as $W(\xi)$ in this case. We will use both notations in what follows.

The functions $W(x, h)$ used as kernels in SPH approximations are required to fulfill the following conditions:

1. $$\lim_{h \to 0} W(x' - x, h) = \delta(x) \tag{27a}$$

2. $$\int_{\Omega} w\,(x' - x, h) dx' = 1 \tag{27b}$$

3. Kernels $W(x' - x, h)$ is positive and has compact support:

$$W(x' - x, h) = 0 \text{ if } |x' - x| \geq kh \tag{27c}$$

where: *k* is a positive integer, which is usually taken as 2.

4. Kernel $W(x' - x, h)$ is a monotonically decreasing function of ξ:

$$\xi = |x' - x|/h \tag{27d}$$

5. Kernel $W(x' - x, h)$ is symmetric function of $(x' - x)$.

The approximation is second order accurate, i.e. $\langle \phi(x) \rangle = \phi(x) + 0(h^2)$

The integral representation of the derivatives in SPH is expressed as

$$\langle \phi'(x) \rangle = \int_{\Omega} \phi'(x') W(x' - x, h) dx'$$

This expression is integrated by parts in 1-D problems and taking into account that the kernel has compact support, it results in

$$\langle \phi'(x) \rangle = -\int_{\Omega} \phi(x') W'(x' - x, h) dx'$$

Classical differential operators of continuum mechanics can be approximated in the same manner. We list below the gradient of a scalar function, the divergence of a vector function and the divergence of a tensor function:

$$\langle \text{grad}\phi(x) \rangle = -\int_{\Omega} \phi(x') \frac{1}{h} W' \frac{x' - x}{r} d\Omega \text{ with } r = |x' - x|$$

$$\langle \text{div u}(x) \rangle = -\int_{\Omega} u(x') \text{ grad } W d\Omega = -\int_{\Omega} \frac{1}{h} W' \frac{u(x').(x' - x)}{r} d\Omega \quad (28)$$

$$\langle \text{div } \sigma(x) \rangle = -\int_{\Omega} \sigma . \text{grad } W d\Omega = -\int_{\Omega} \frac{1}{h} W' \frac{\sigma.(x' - x)}{r} d\Omega$$

These are obtained by the application of integral theorems and taking into account that kernels have compact support.

2.5 Parametrizing DAN3D model

Input files used in DAN3D simulations were topography files in ASCII format. Path topography file: where the grid file represent surface of slide mass flow. The second one is source depth topography file that is also called release area and it is the vertical depth file of the slide mass at initial conditions. Both of them should be prepared in DEM form. Preparation of the DEM was done using Surfer-11 and ArcGIS-10.2.2 soft wares.

DAN3D model has the following parameters; material properties and control parameters.

Material properties; these parameters include unit weight, shear strength, viscosity, types of rheology and friction and internal friction angle (Figure 11). There are other parameters in

the material property but these are the one, which are considered during running the model. Simulation of the model was running according to the parameters indicated in Table 1.

Control parameters; these include model time and time stepping.

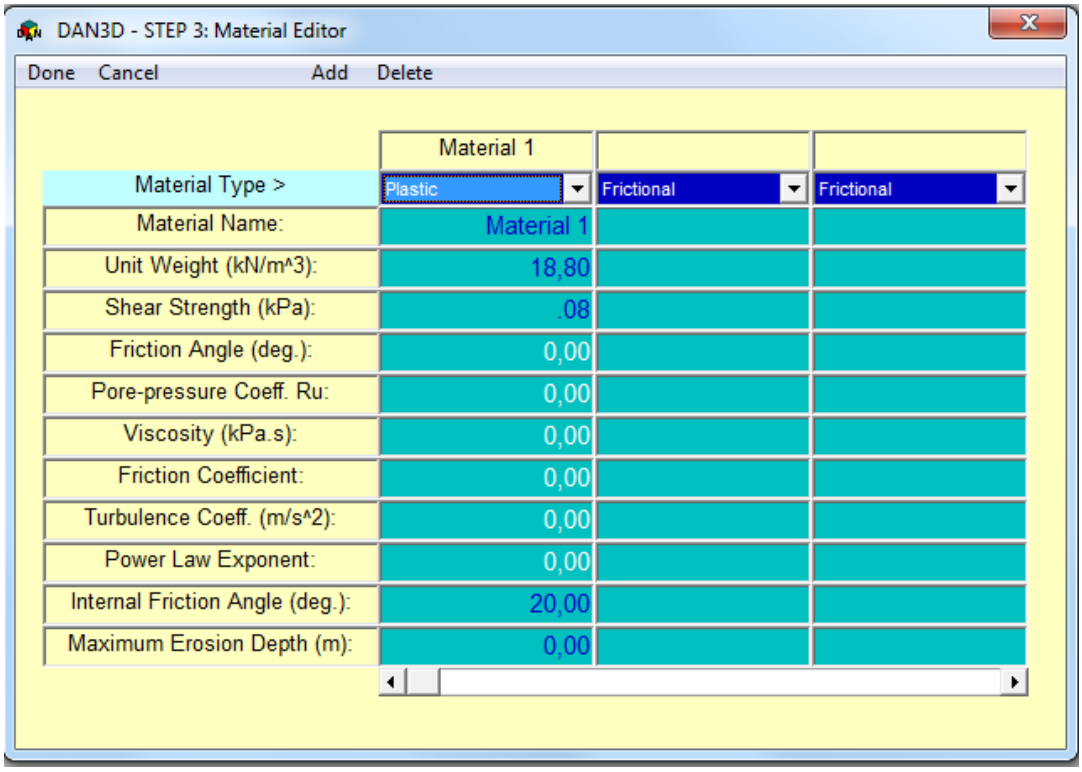

Figure 11: DAN3D input parameters using plastic rheology for Finneidfjord landslide. Values shown in blue colour are considered in the simulation of the model.

Table 1: Input parameters for both of the models (DAN3D and BING).

Material properties	Finneidfjord slide
Types of rheology	Plastic & Bingham
Unit weight (kN/m^3)	18.8
Shear strength (kPa)	0.08
Viscosity (kPa.s)	7.85x10^{-3}
Internal friction angle (degree)	20

Sources: Natterøy, (2011), Issler et al., (2012) and Nigussie, (2013).

3. Simulation results of the models

3.1 Introduction

Simulation results of both DAN3D and BING models are presented in this section. It was done for both synthetic benchmarking and Finneidfjord landslide cases. The detail simulations were done as follow;

Before running the DAN3D model, it is very important you have to define the topography of the study area as DEM, define the source depth and select the appropriate rheology based on the information of landslide that occurred. The planar topographic surface and release area of Finneidfjord area are shown in Figure 12. As this was mentioned in Issler et al., (2012), DAN3D is not account for buoyancy during the simulation of submarine slide. Therefore, adjustment was made on the bathymetry of the submarine surface to reduce the effect of buoyancy. Buoyancy reduces the gravitational force in water by a factor $1 - \rho_w/\rho_q \approx 0.48$ but the other forces remain the same.

In order to run BING, one has to define the geometry of initial length, maximum thickness of the slide and tail of slide. Bed files profile was also created in ArcGIS from the DEM and used as input for the simulation of the model. The data was exported to spreadsheet as text file that contain slope distance and elevation at an arbitrary datum.

The BING model was simulated using Herschel-Bulkley rheology at a limiting case, $n = 1$, that is Bingham rheology and compared the results with DAN3D for both synthetic benchmarking and Finneidfjord landslide. It was simulated with the same parameters like DAN3D model. Synthetic DEM for benchmarking was also used to understand the model by defining a grid size of 25x25 m^2 with slope of 5^0.

The different simulation results are presented in section 3.2 for the synthetic benchmarking case and section 3.3 for Finneidfjord landslide using both plastic and Bingham rheology. In addition to these, comparison between BING and DAN3D for both the synthetic benchmarking and Finneidfjord landslide was taking into consideration and result of simulations are presented in this section.

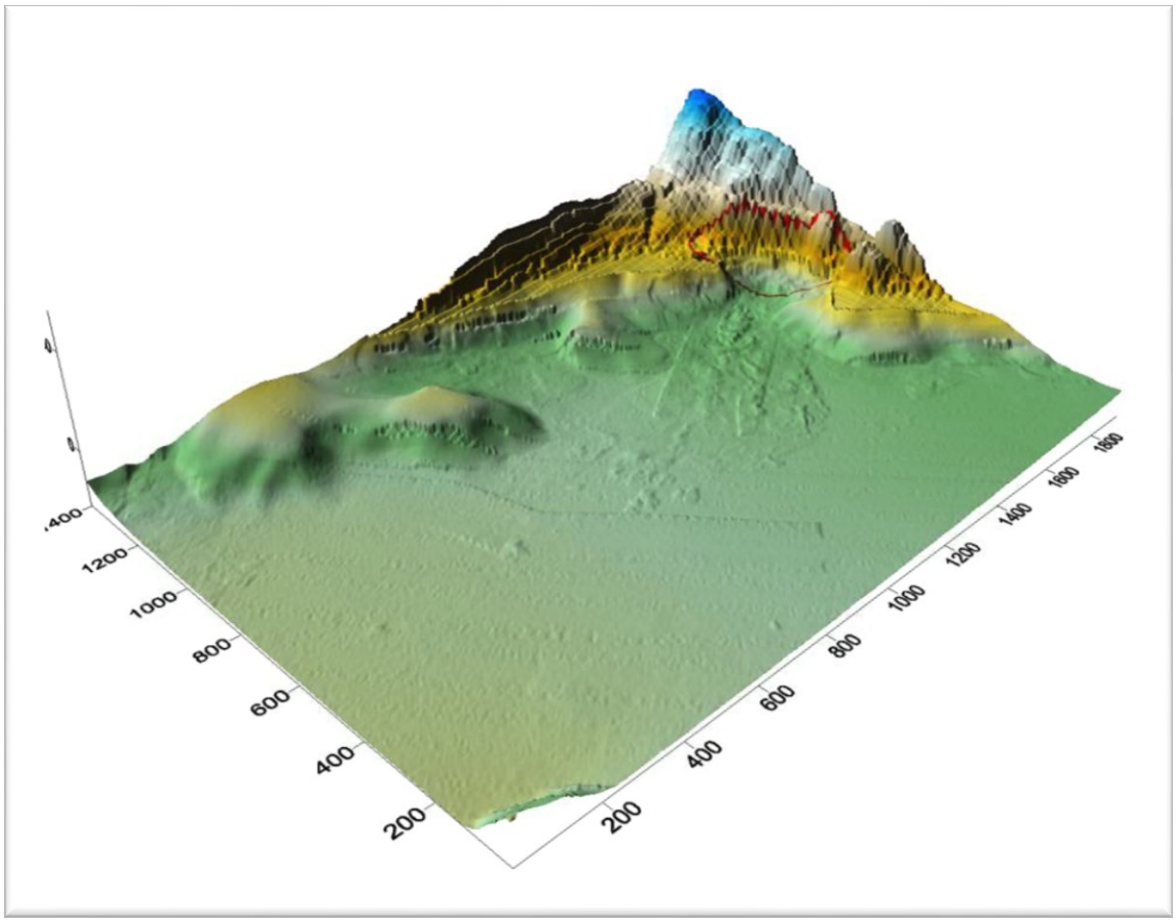

Figure 12: Three-dimensional topographic surface of Finneidfjord area, release area of the slide mass is indicated in a circular shape with red color line.

Profile graph has been prepared from the DEM of the Finneidfjord landslide area. One of the profile graph shows along the movement of the slide and the second one is across the slide (Figure 13). This was done to check the topography of the study area after mosaicking the DEM from the Finneidfjord side and the land. Beside to this, flow direction and flow accumulation was prepared to control the quality of the DEM of the study area. The color of the lines (Figure 13) indicates that the locations where the surface is visible (green) and where it is hidden (red) from an observer (Help ArcGIS).

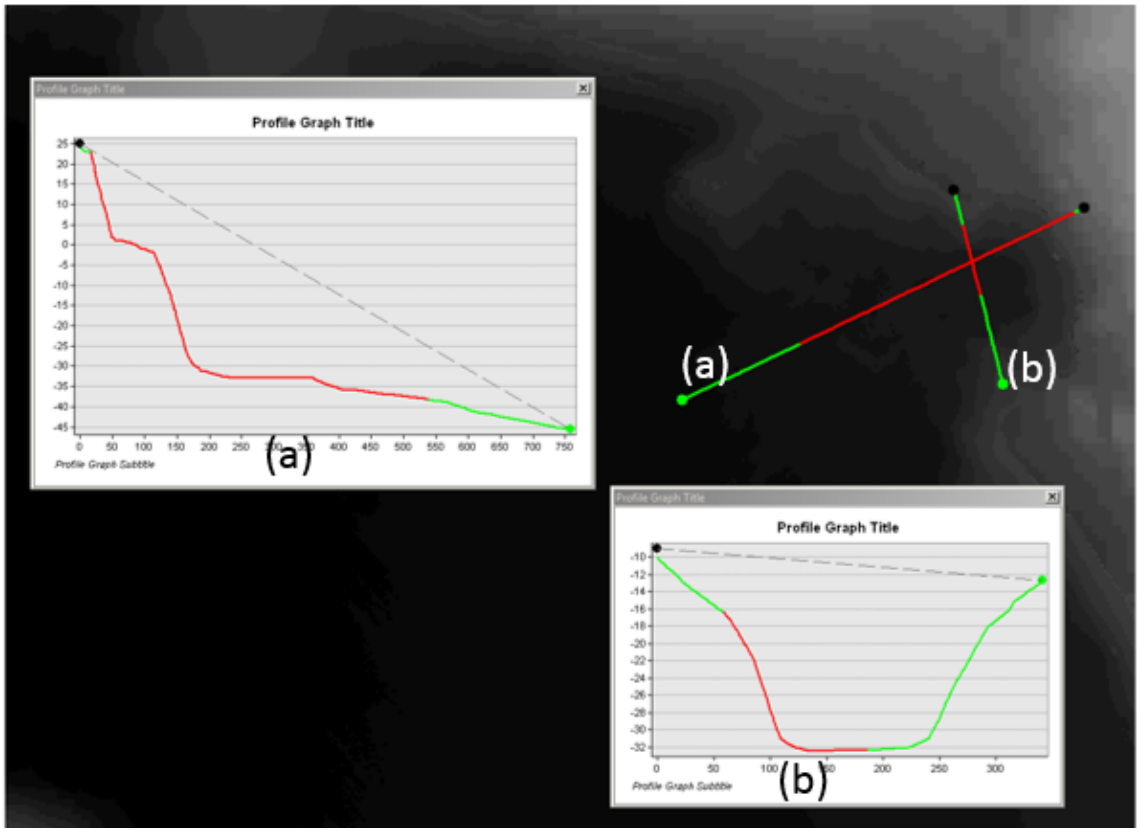

Figure 13: Cross sectional view of Finneidfjord landslide along the slide (movement direction) (a) and across the movement of slide (b) prepared from DEM.

3.2 Benchmarking

3.2.1 DAN3D model

In simulation of numerical model, the first step is to ensure that the model is able to provide accurate results for the analyses (Blanc et al., 2011). Synthetic DEM for benchmarking is helping to control the quality of the simulation and understand the result of the model. To do this, it has to define geometry for the synthetic benchmarking, prepare the geometry in excel sheet and import to surfer for further analysis in the model.

We have defined a path topography with a grid area of 25x25 m^2 taking points of x, y and z in excel sheet in columns. Beside to this, we have also defined the source topography with slope of 5^0. After defining these topographies and taking as input for DAN3D, the simulation was running using both plastic and Bingham rheologies with the same parameters as in the case of Finneidfjord landslide (Table 1). The analysis result of the simulation for flow distance and flow velocity against simulation time using plastic rheology are shown in

Figure 14 and Figure 15. Bingham rheological simulation was also done and the results are shown in Figure 16 and Figure 17.

As it is shown in Figure 14 and Figure 15, the process of moving and stopping the simulation was clear and it has defined time of runout distances however, when we see both Figure 16 and Figure 17, they look different especially in the case of runout it has not an end point (see Figure 16). These differences occurred when the model used different rheology, in this case plastic and Bingham rheology.

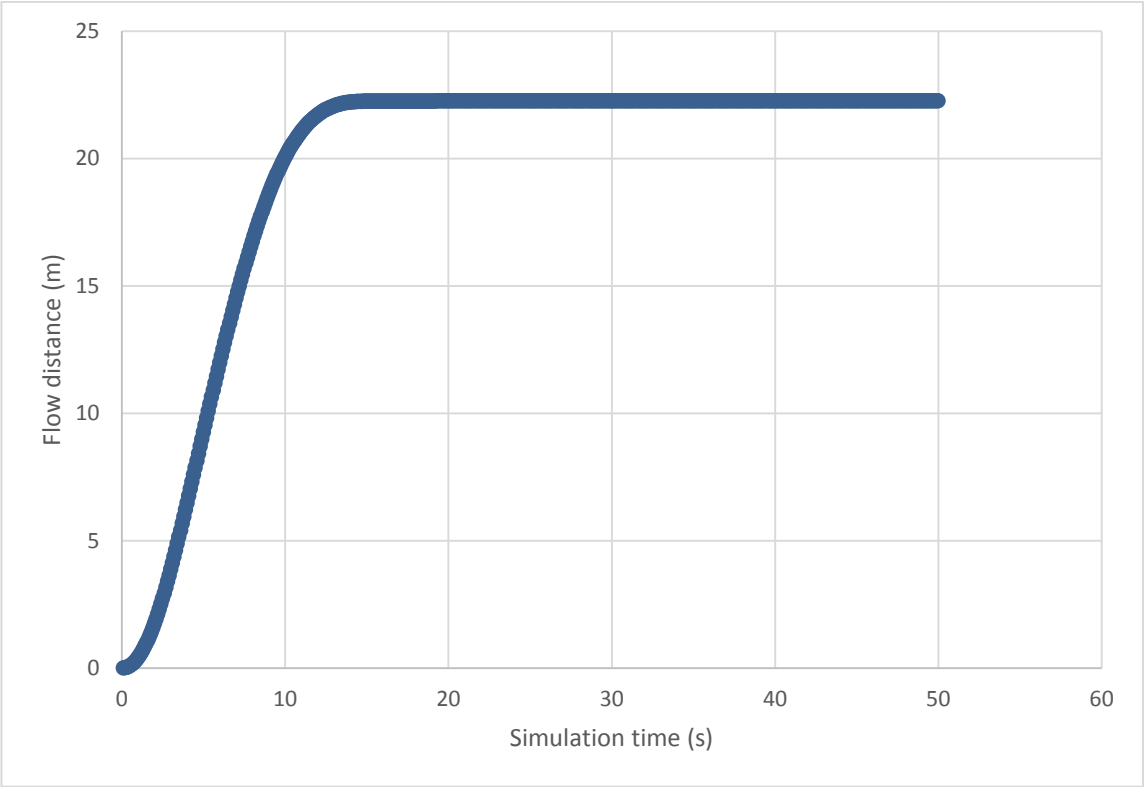

Figure 14: Analysis of the benchmark using plastic rheology for flow distance vs. simulation time.

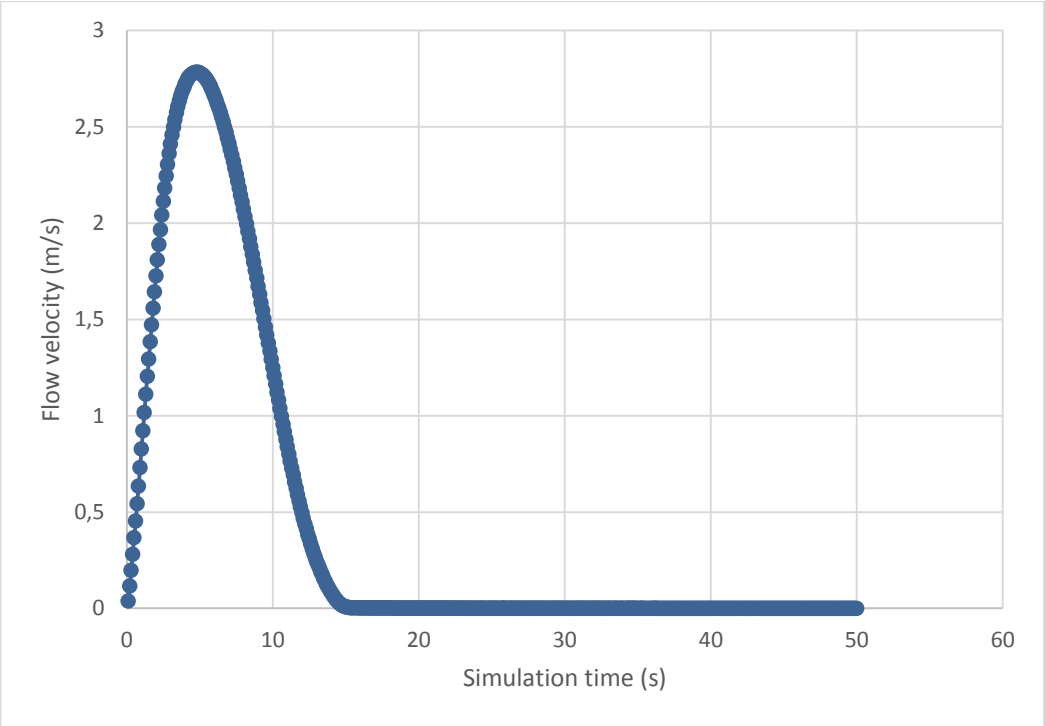

Figure 15: Analysis of the benchmark using plastic rheology for flow velocity vs. simulation time.

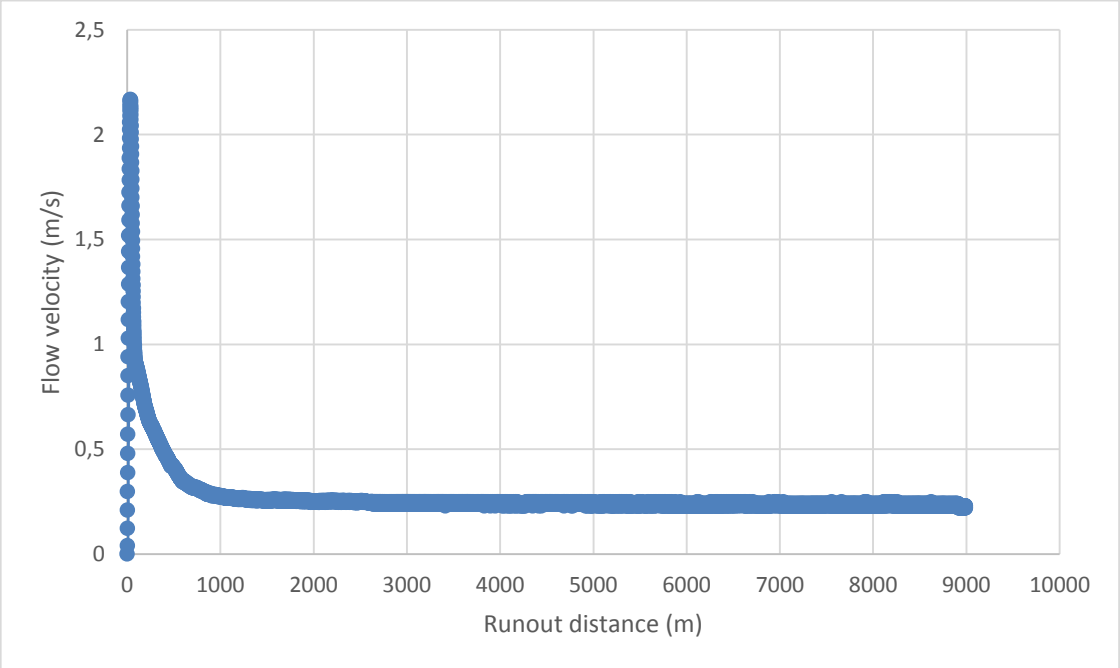

Figure 16: Analysis of the benchmark using Bingham rheology for flow velocity vs. runout distance.

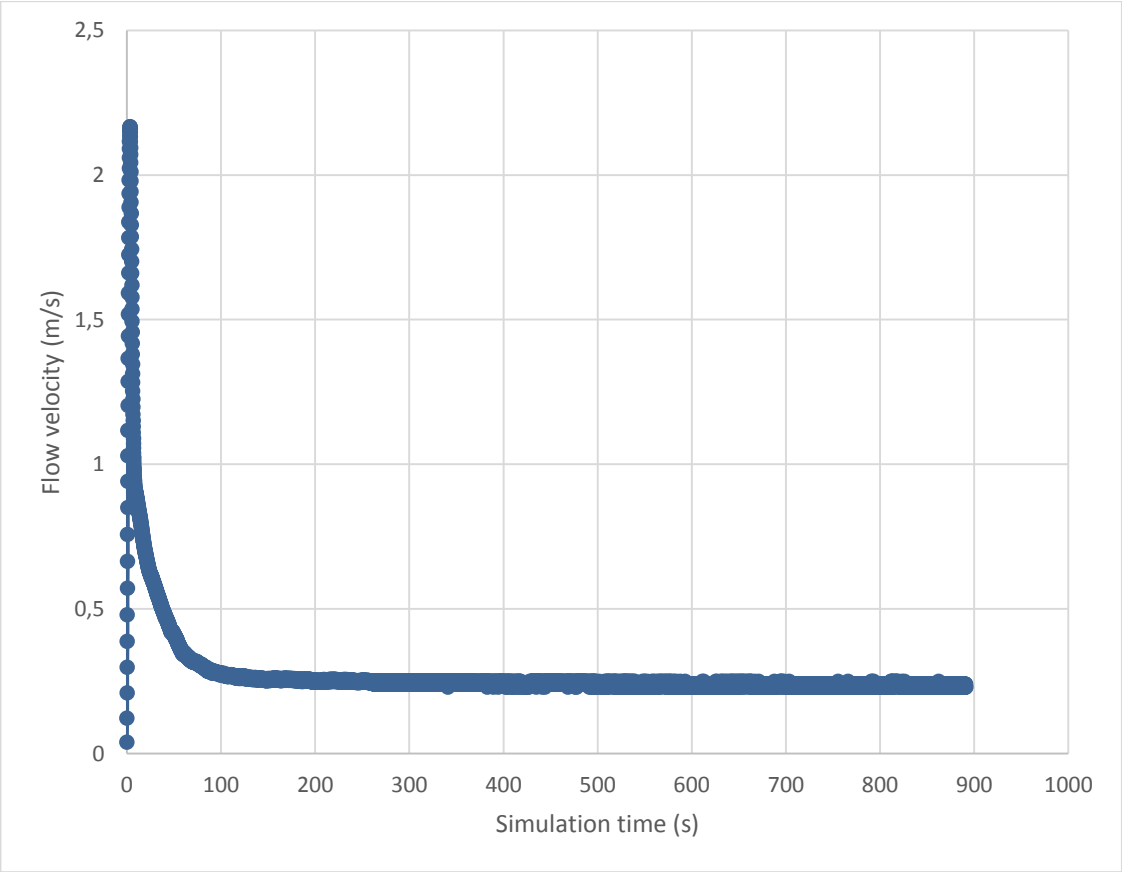

Figure 17: Analysis of the benchmark using Bingham rheology for flow velocity vs. simulation time.

3.2.2 BING model

BING model was simulated using the same parameter like DAN3D-Finneidfjord landslide case (Table 1). Some of the running results are displayed in Table 2. As it is shown in Table 2, the runout distances and peak front velocities have different values based on the number of nodes and artificial viscosity. We have used for further analysis one of the simulation results (Run no. 1). The graph is drawn using flow velocity vs. simulation time (Figure 1). This graph has shown the process of moving and stopping of simulation. The ranges of runout distance and peak front velocities are shown in Table 2. Comparison of runout distances and flow velocities were made for both models as presented in Figure 19, Figure 20 and Figure 21.

Table 2: BING Rheological and numerical values used to run Bingham rheology for the benchmarking.

Run no.	γ_r	γ	n	ρ_q	ρ_w	No of nodes	Artificial viscosity	Runout (m)	Max. Front Velocity (m/s)
1	10.2	800	1	1880	1000	10	0.0001	18.671	5.151
2	10.2	800	1	1880	1000	10	0.001	18.657	5.139
3	10.2	800	1	1880	1000	21	0.001	18.467	4.756
4	10.2	800	1	1880	1000	21	0.01	18.464	4.779
5	10.2	800	1	1880	1000	40	0.001	18.255	4.744
6	10.2	800	1	1880	1000	45	0.0001	18.254	4.756

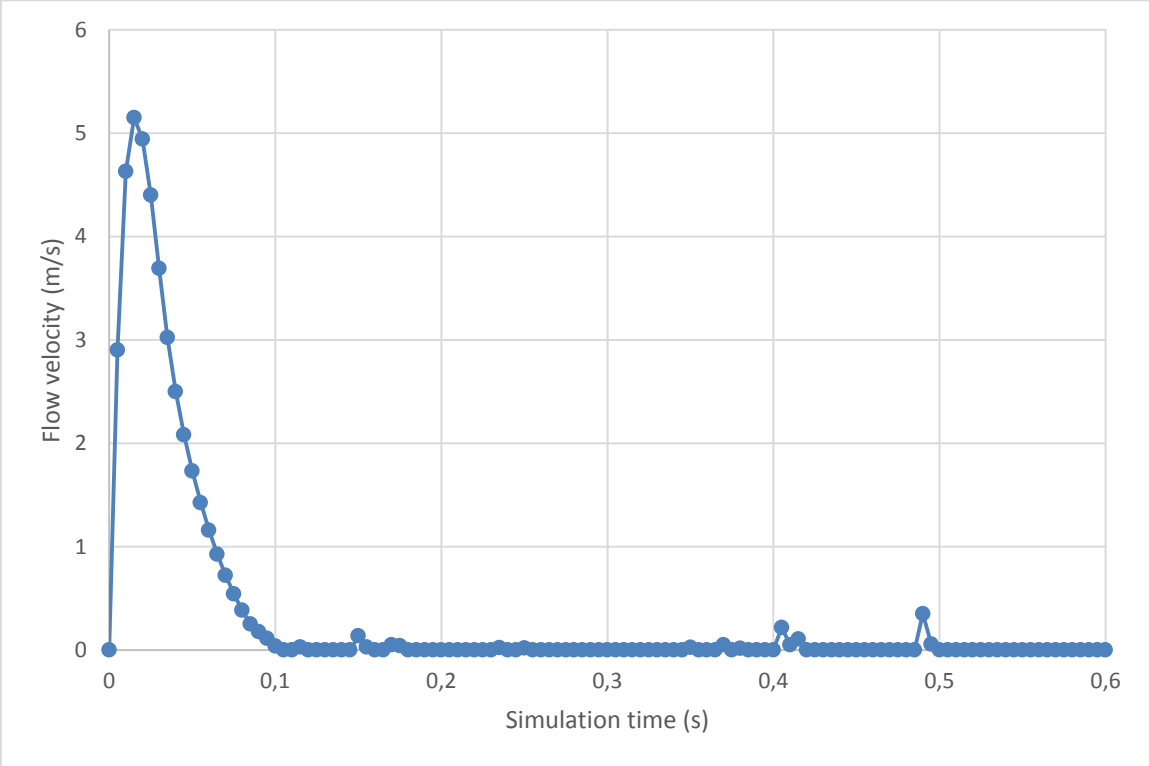

Figure 18: Analyses of flow velocity vs. time using BING model (Run no. 1 in Table 2).

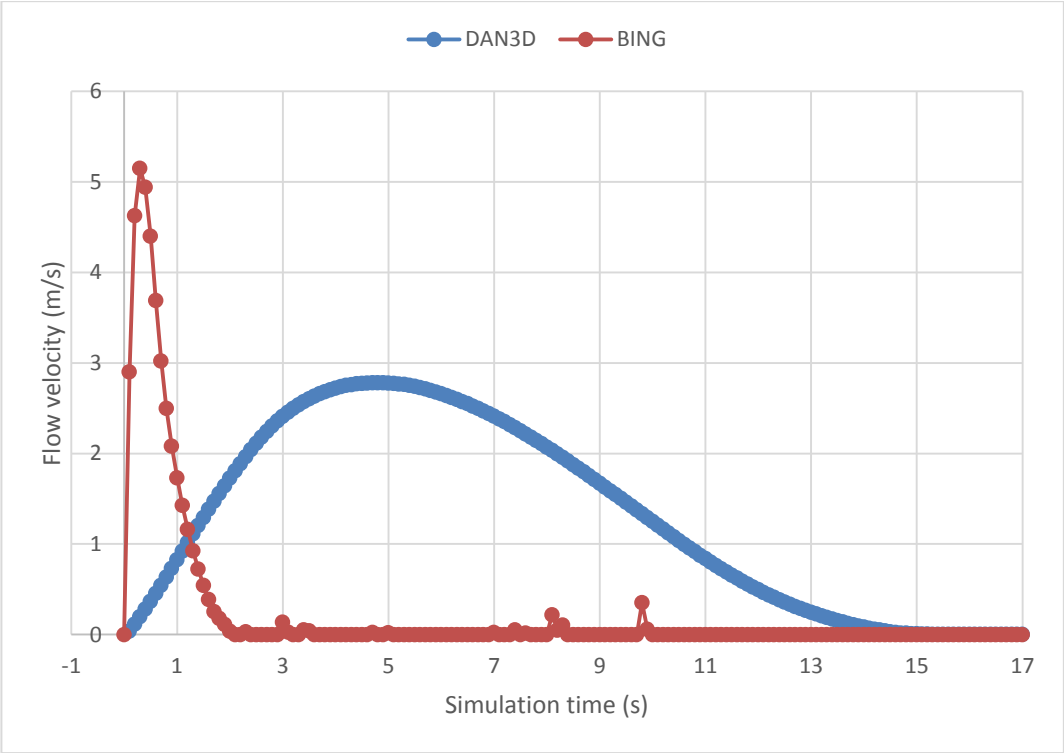

Figure 19: Analysis of flow velocity vs. time using both DAN3D (plastic) and BING model.

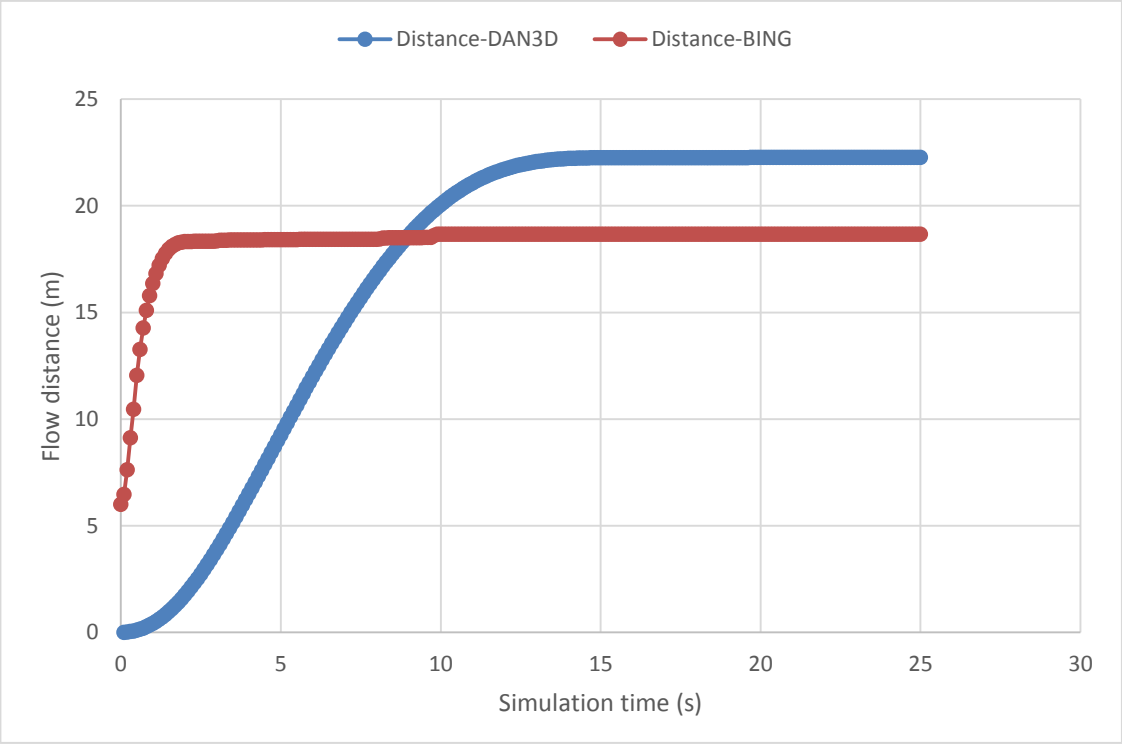

Figure 20: Comparison of flow distance vs. simulation time using both DAN3D and BING models.

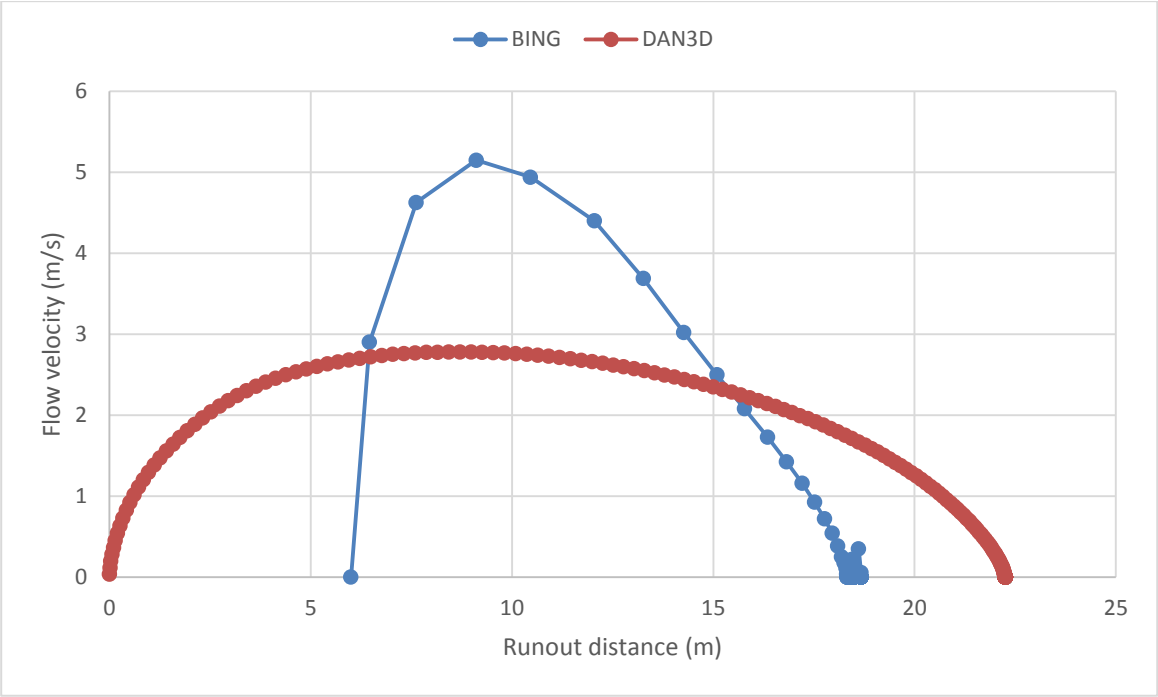

Figure 21: Analysis of both DAN3D (plastic rheology) and BING models.

3.3 Finneidfjord landslide

3.3.1 DAN3D model

3.3.1.1 Simulation of the model using plastic rheology

Simulation of plastic rheology was done using the value of the remoulded shear strength of 0.08 kPa (Natterøy, (2011), L'Heureux et al., (2012) and Issler et al., (2012)). The simulation was done with maximum and minimum volume slides 1,220,000 m^3 and 945,000 m^3 respectively. These volumes were taken from Issler et al., (2012) by considering and summing up the minimum and maximum in the three main stage of Finneidfjord landslides (945,000 m^3 − 1,220,000 m^3).

3.3.1.1.1 Simulation of maximum volume of release area (1,220,000 m^3)

The following maps (Figure 22) have shown the simulation result of the model for the flow distance and flow thickness of the deposit at different simulation time. The contour maps showed the variation of deposits at different stage of simulation time. The red lines in the maps showed the source area of slide. The simulation time ranges from 50 to 400 seconds.

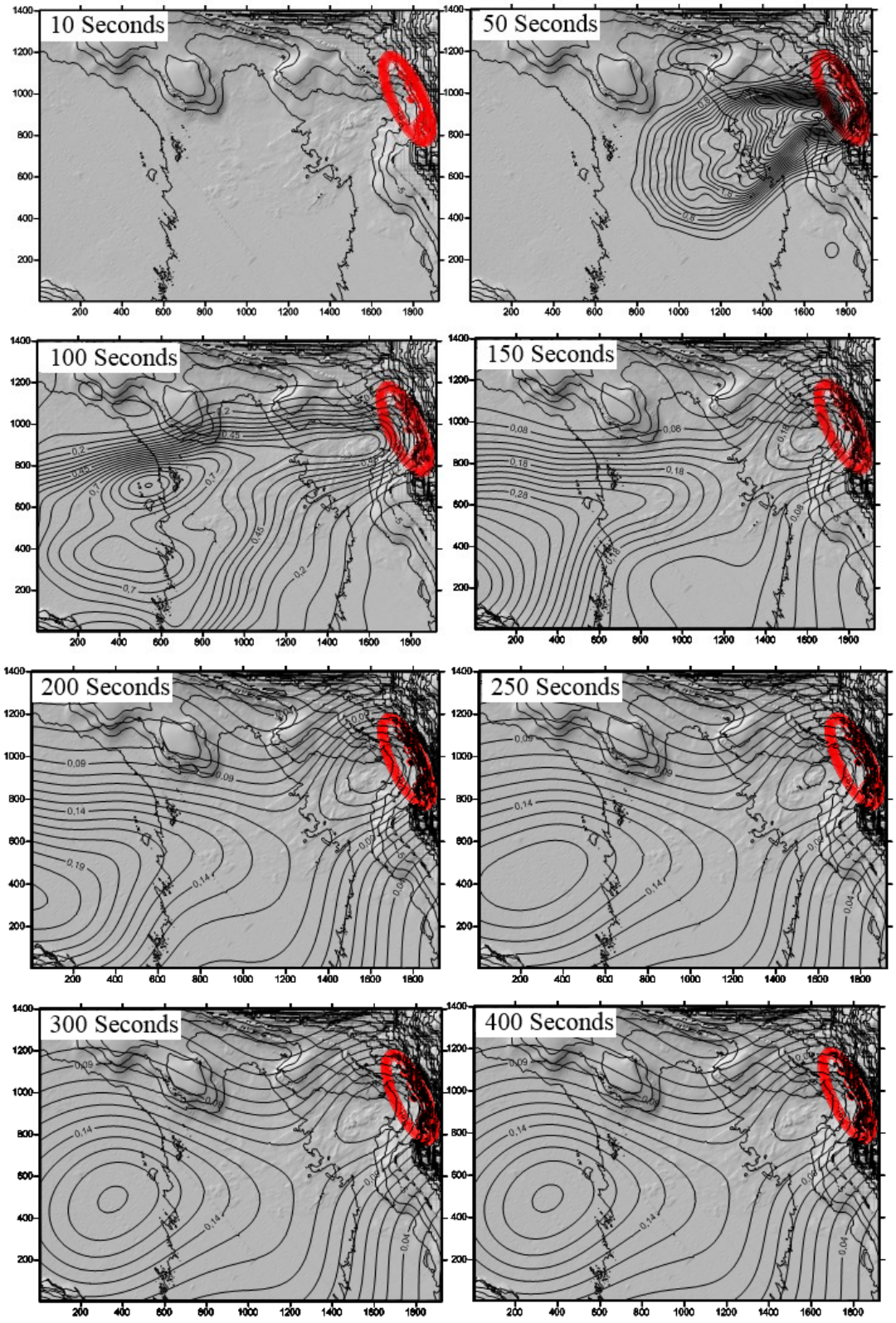

Figure 22: Flow thickness contours at 10, 50, 100, 150, 200, 250, 300 and 400 simulation time (seconds) for the maximum volume using plastic rheology.

Using the output files of simulations, graph of flow distance vs. time was prepared and it is shown in Figure 23. Flow velocity vs. time was also presented and displayed in Figure 24. Figure 25 shows the maximum velocity in the simulation.

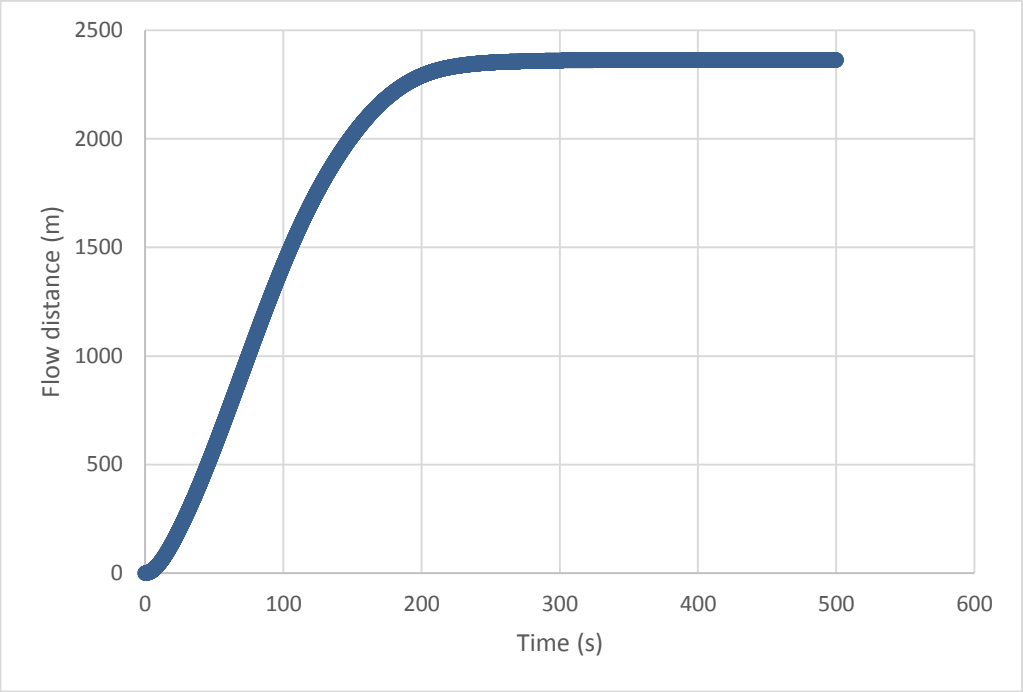

Figure 23: Analysis of flow distance vs. simulation time.

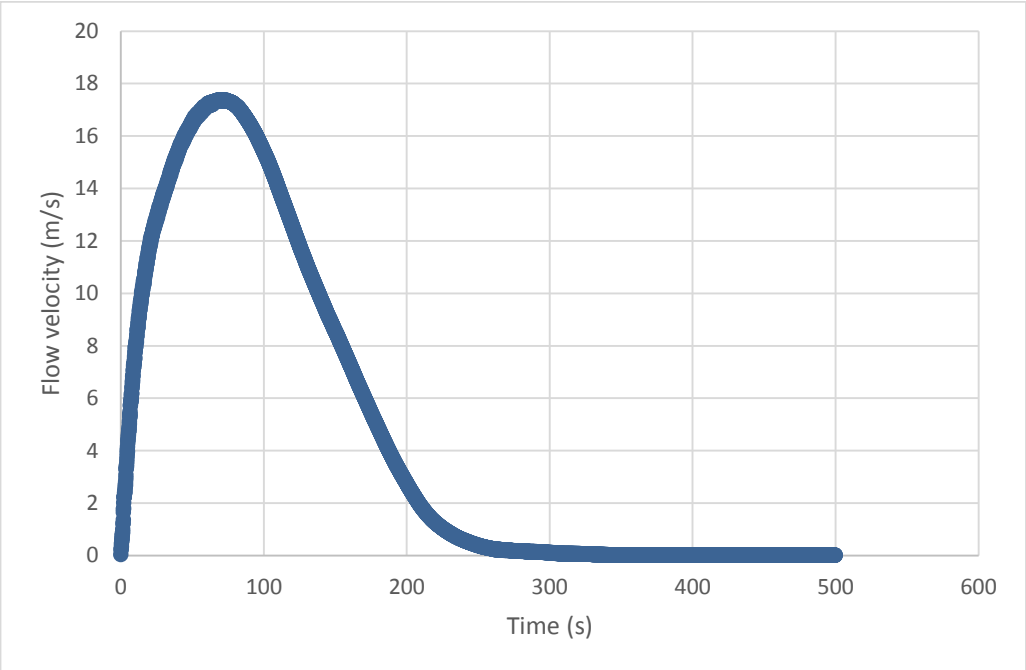

Figure 24: Analysis of flow velocity vs. simulation time.

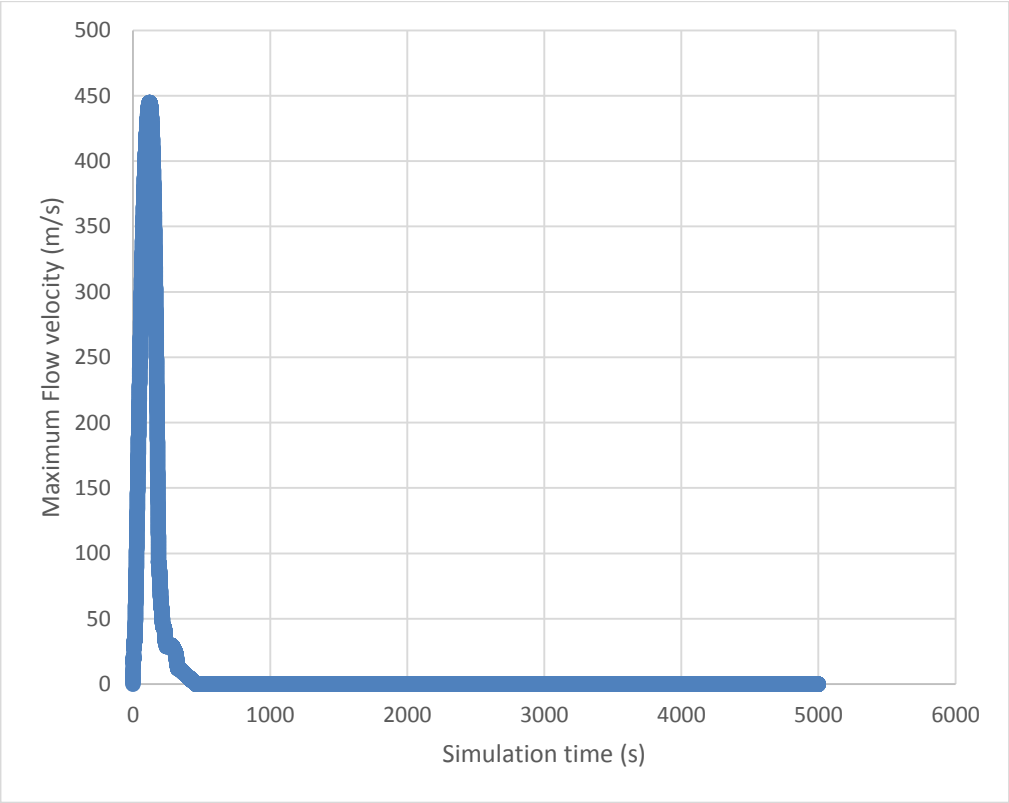

Figure 25: Maximum flow velocity vs. simulation time of the model.

3.3.1.1.2 Simulation of minimum volume of release area (945,000 m^3)

Figure 26 indicates the simulation result of the model for the flow distance and flow thickness of the deposit at different simulation time for the minimum volume of the slide. The map showed variation of flow thickness and deposit of the slide within the study area. The red colour contours are the release area of the slide. Contours starting from the source area (red contour lines) show flow distance and deposit of the slide during simulation of the model. These contours are flowing in the direction of southwest of the study area (Figure 26). After analysing the simulation output files, it has prepared runout distance vs. time, flow velocity vs. time, and maximum velocity of the simulation as it is shown in Figure 27, Figure 28 and Figure 29 respectively. In addition to the above, a graph was prepared to compare both volumes using the same rheology (Figure 30).

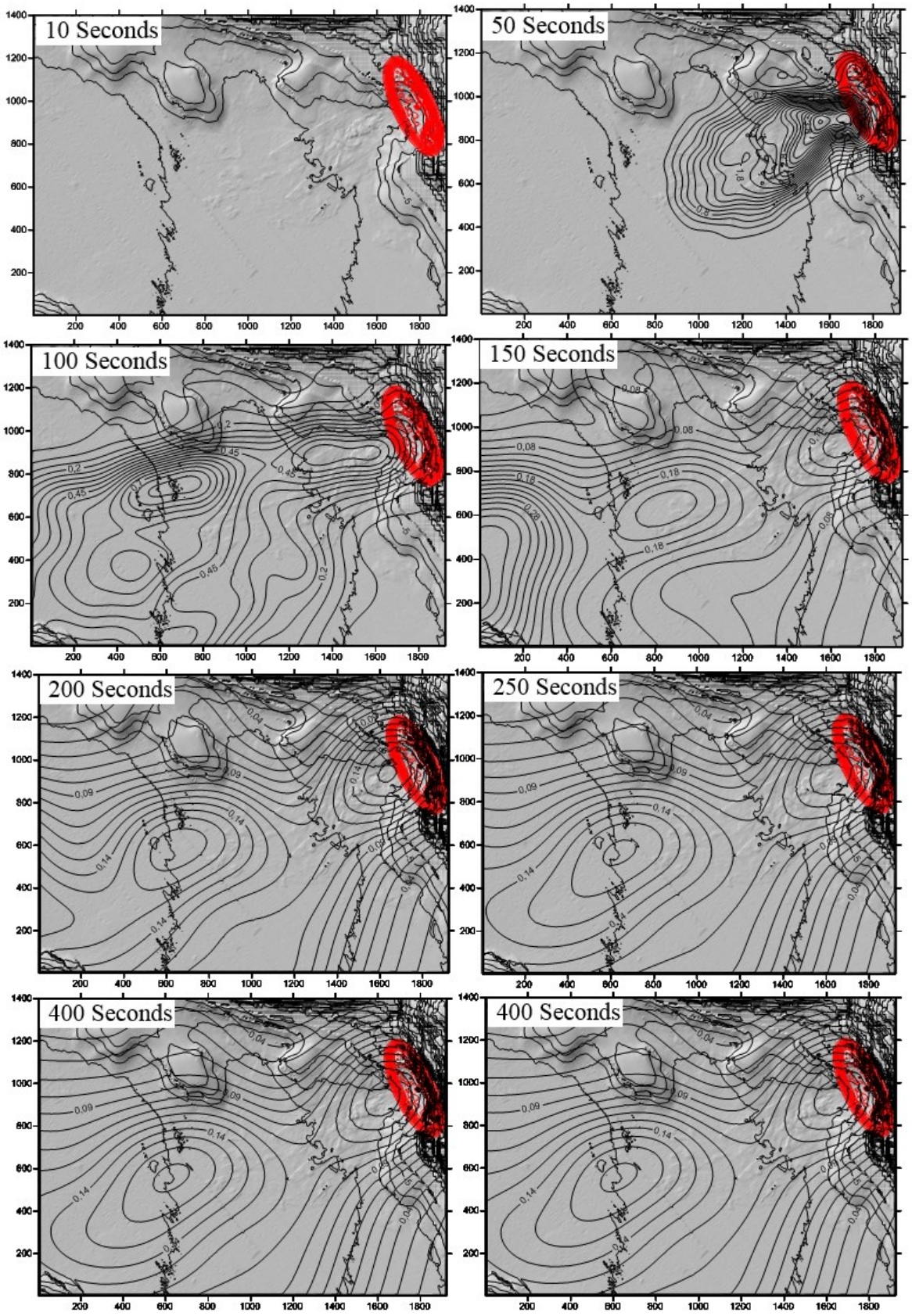

Figure 26: Flow thickness contours at 10, 50, 100, 150, 200, 250, 300 and 400 simulation time (seconds) for the minimum volume using plastic rheology.

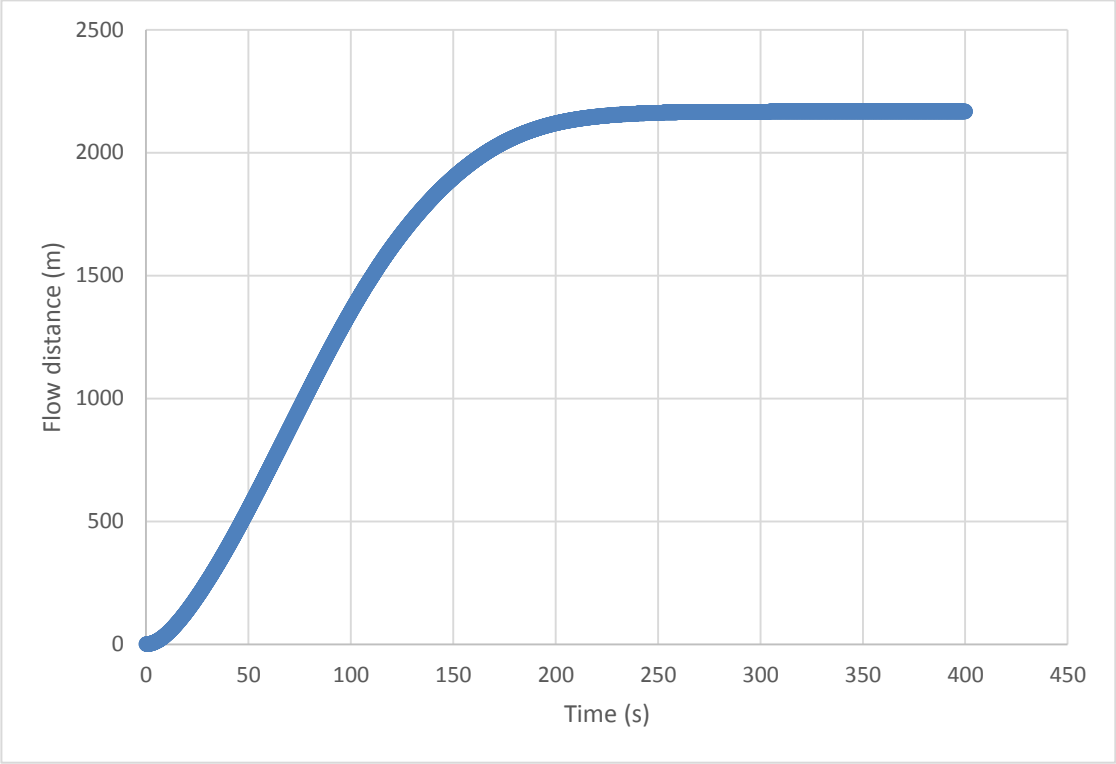

Figure 27: Analysis of flow distance vs. simulation time.

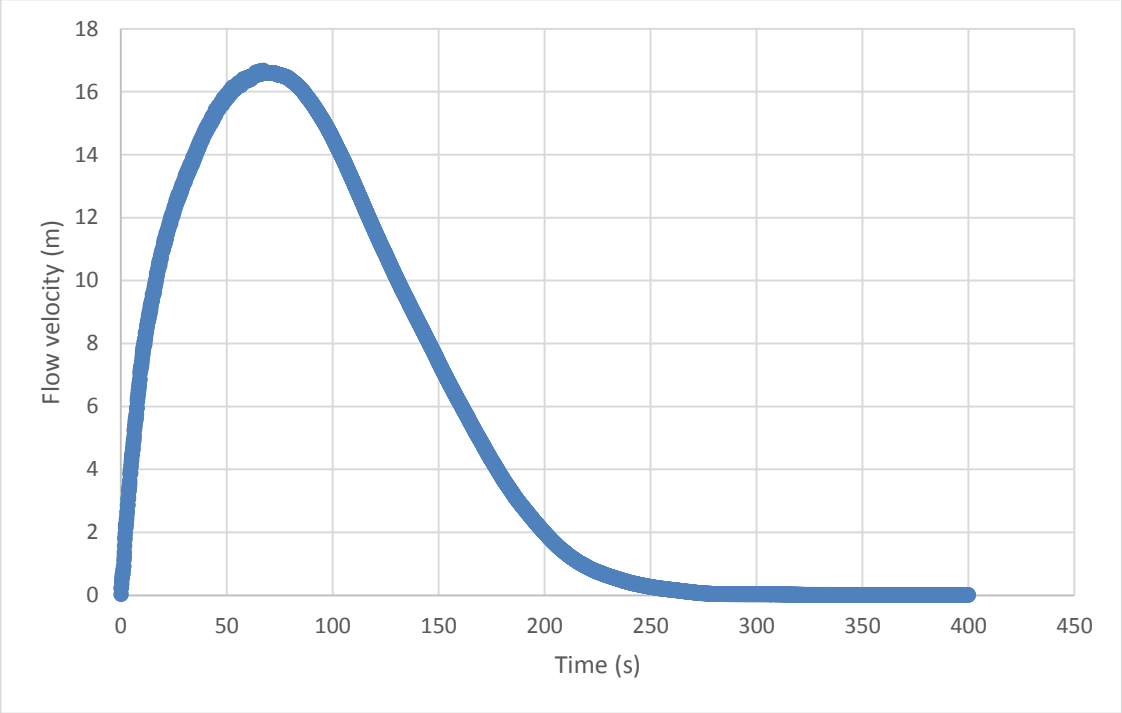

Figure 28: Analysis of flow velocity vs. simulation time.

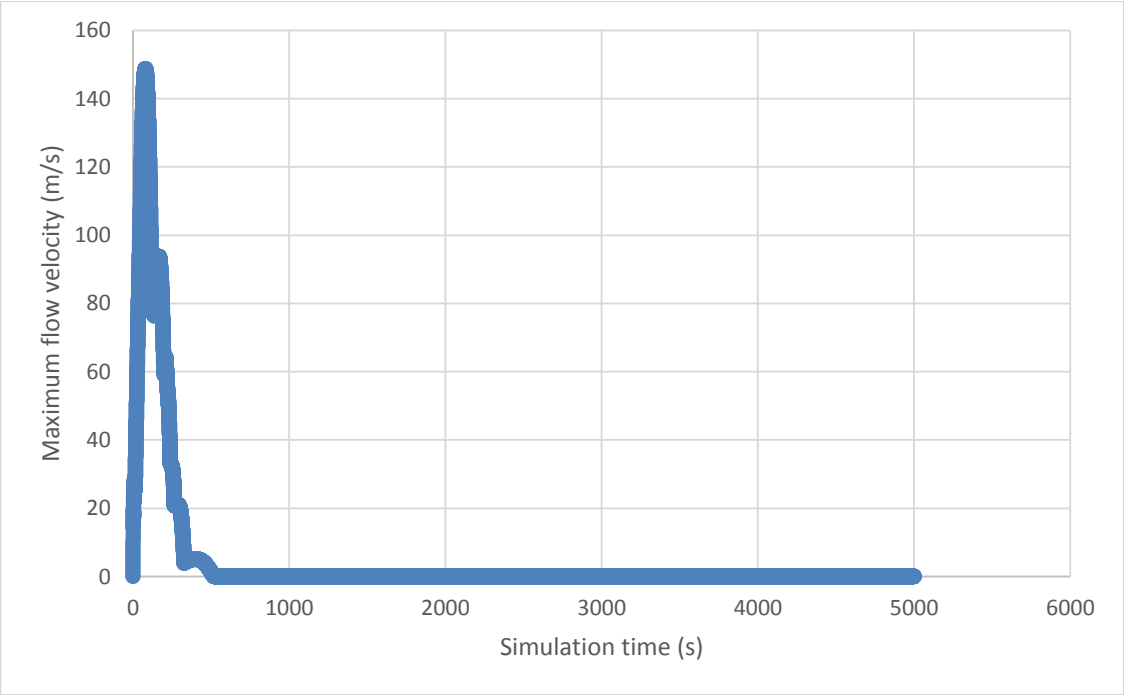

Figure 29: Maximum flow velocity vs. simulation time of the model.

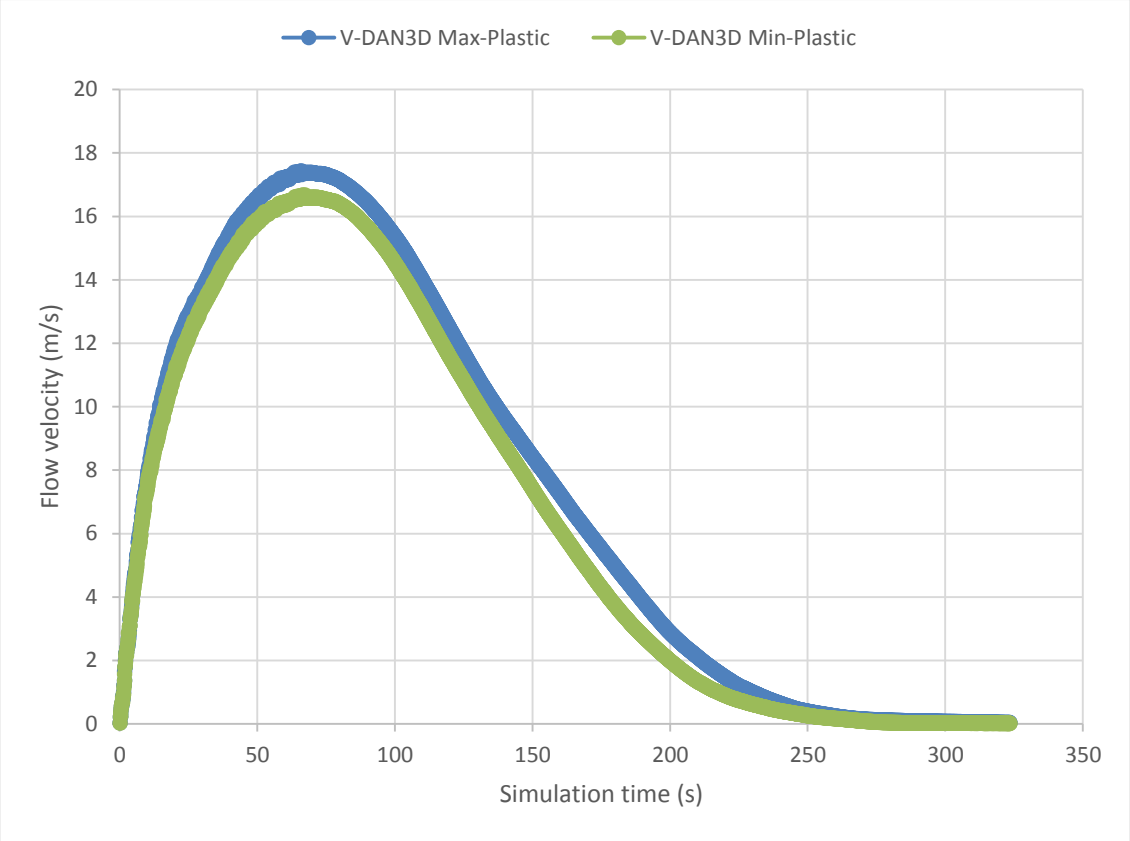

Figure 30: Comparing both volumes using plastic rheology (flow velocity vs. time).

3.3.1.2 Simulation of the model using Bingham rheology

Simulation of Bingham rheology was also done using the same value of remoulded shear strength as in the case of plastic rheology above. It was done with the same parameters as in the case for plastic simulation (section 3.3.1.1). In addition to the plastic parameter, Bingham rheology simulation used dynamic viscosity. The value of the remoulded shear strength was 0.08 kPa (Natterøy, 2011) and (Issler et al., 2012) and the dynamic viscosity was 7.85×10^{-3} kPa.s (Nigussie, 2013). Besides to these parameters, internal friction angle is also another element that was considered in simulation of the model. The analysis result of the flow distance and flow velocity of the simulation are presented in the next sections.

3.3.1.2.1 Simulation of maximum volume of release area (1,220,000 m^3)

Bingham rheological simulation was done and the results are shown in Figure 31 for different simulation time of the model. Simulation time ranges from 50 to 3,000 seconds. Flow contours shown in Figure 31 represent thickness of the deposit and how far it is located form the source area. Red line in the maps shows the location of the source area. The flow direction is from the source towards southwest of the study area. Flow distance and velocity vs. time have presented in Figure 32 and Figure 33 respectively.

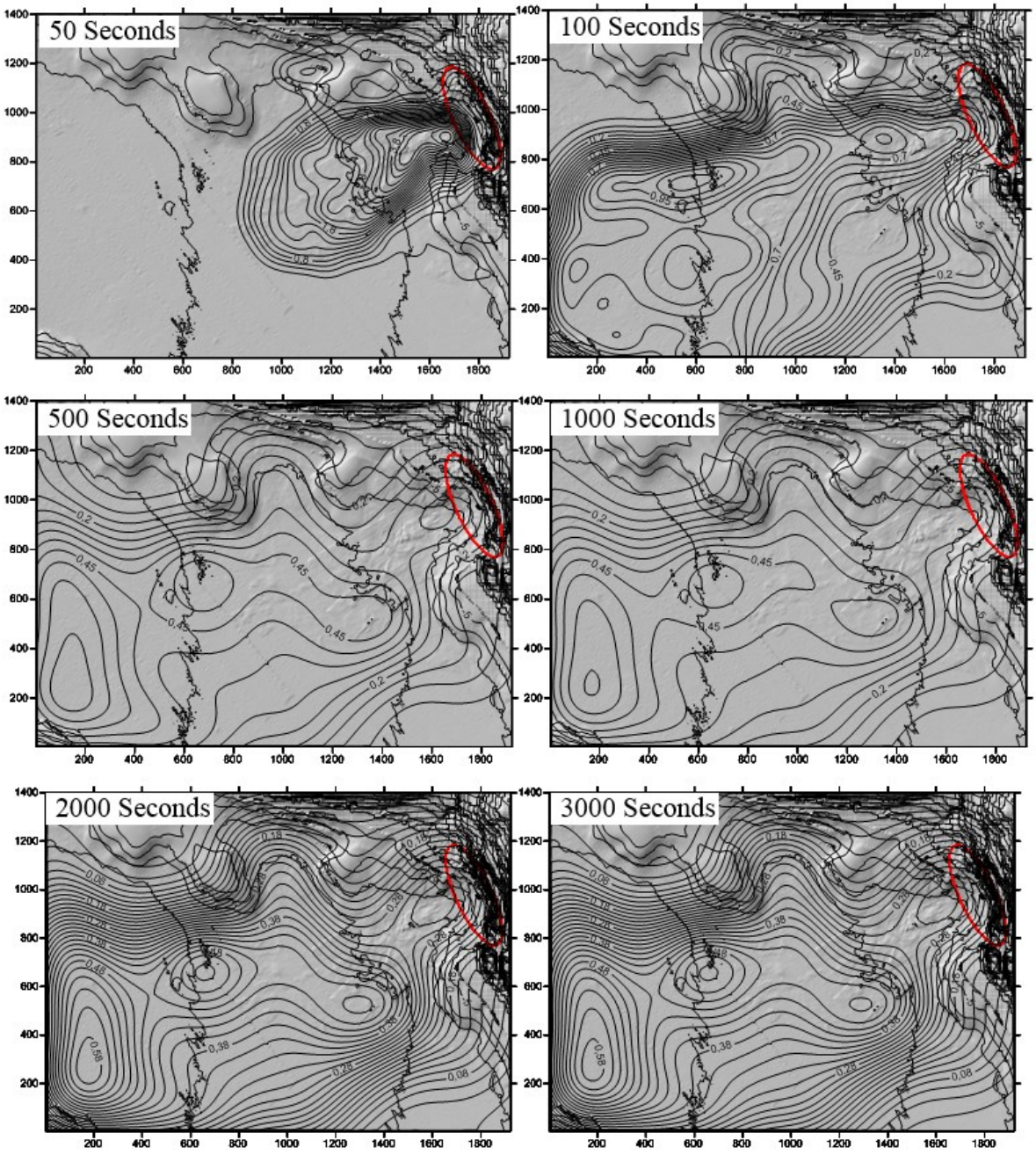

Figure 31: Flow thickness contours at 50, 100, 500, 1000, 2000 and 3000 simulation time (seconds) for the maximum volume using Bingham rheology.

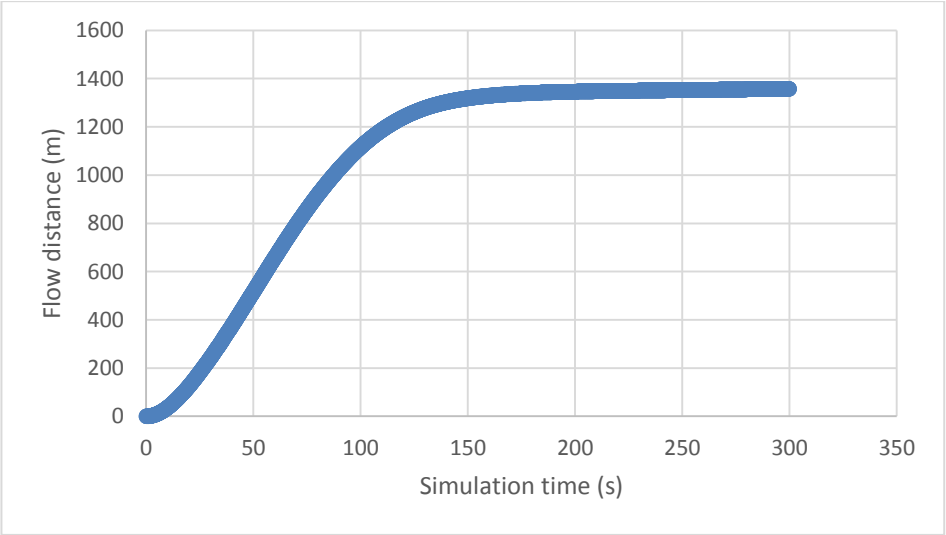

Figure 32: Analysis of flow distance vs. simulation time.

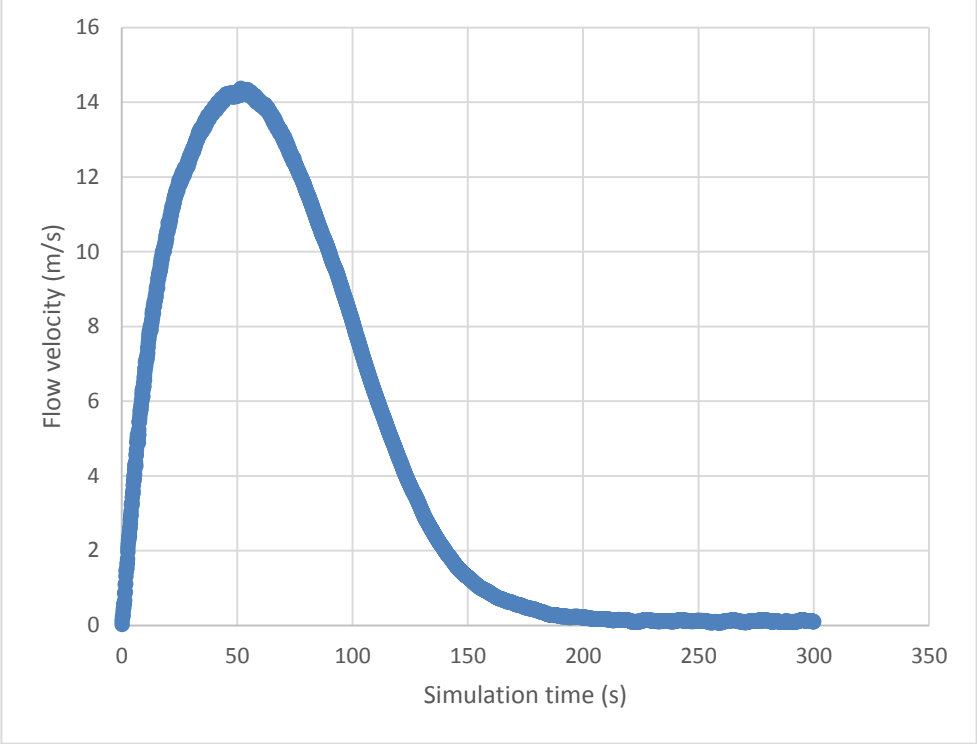

Figure 33: Analysis of flow velocity vs. simulation time.

3.3.1.2.2 Simulation of minimum volume of release area (945,000 m^3)

Simulation was also done for the minimum volume slide. The results of the simulation are shown in Figure 34. The simulation results ranges from 50 to 50,000 seconds. Flow contours are shown at different simulation time and the red line represent source area for the slide.

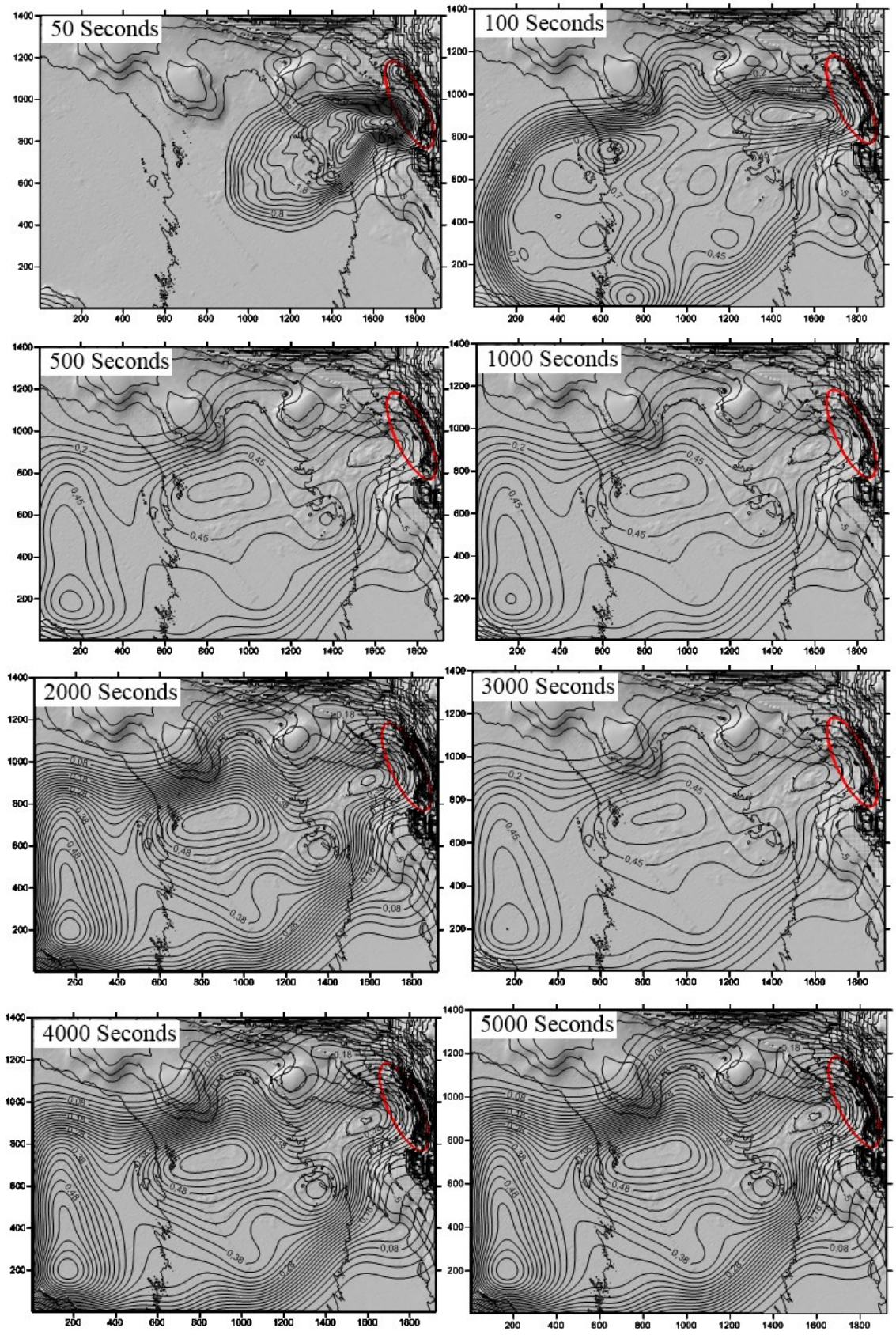

Figure 34: Flow thickness contours at 50, 100, 500, 1000, 2000, 3000, 4000 and 5000 simulation time (seconds) for the minimum volume using Bingham rheology.

To observe the behaviour of simulation, an analysis was done for flow distance (Figure 35) and flow velocity (Figure 36). Figure 38 and Figure 37 were used the same data as Figure 35 and Figure 36 respectively but the only difference is that the latter case used more data. Both volumes were simulated to see the difference in flow velocity (Figure 39). Similarly, both volumes and rheologies were analysed their flow distances and these showed which one run fast and vice versa (Figure 40). Flow velocity was also analysed and this is shown in Figure 41.

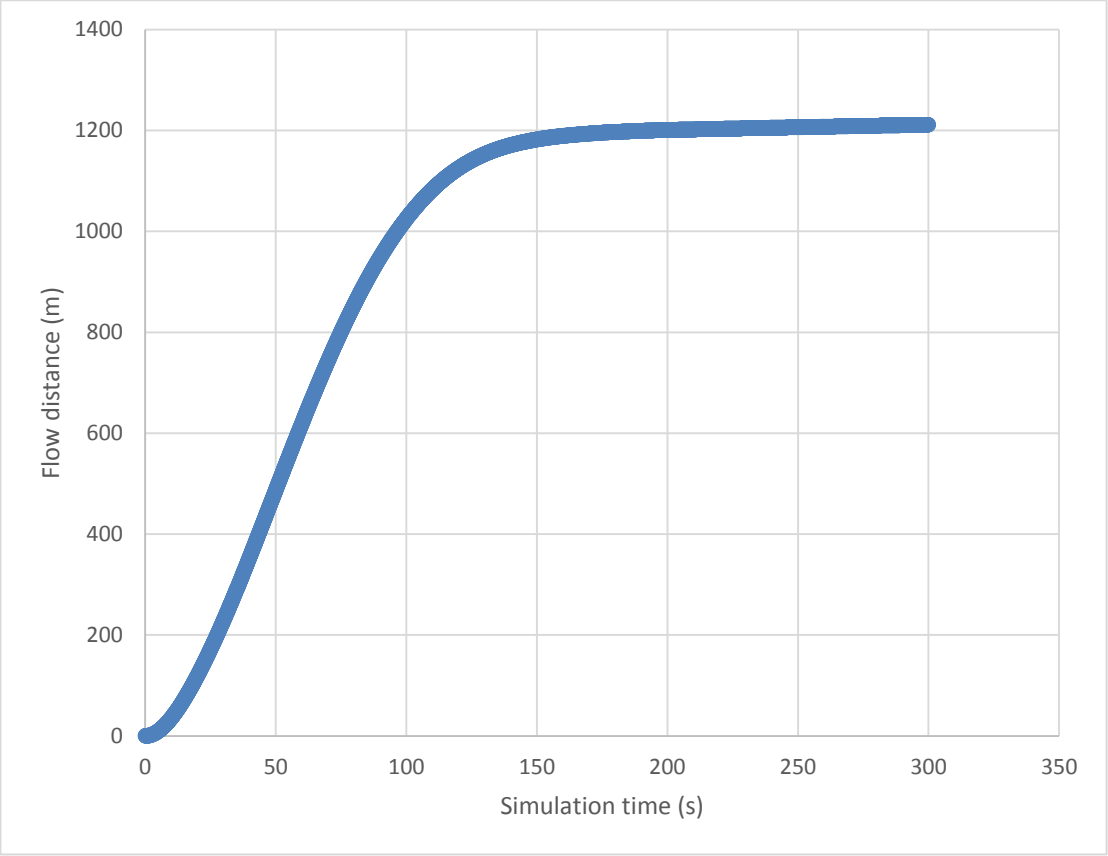

Figure 35: Analysis of flow distance vs. simulation time.

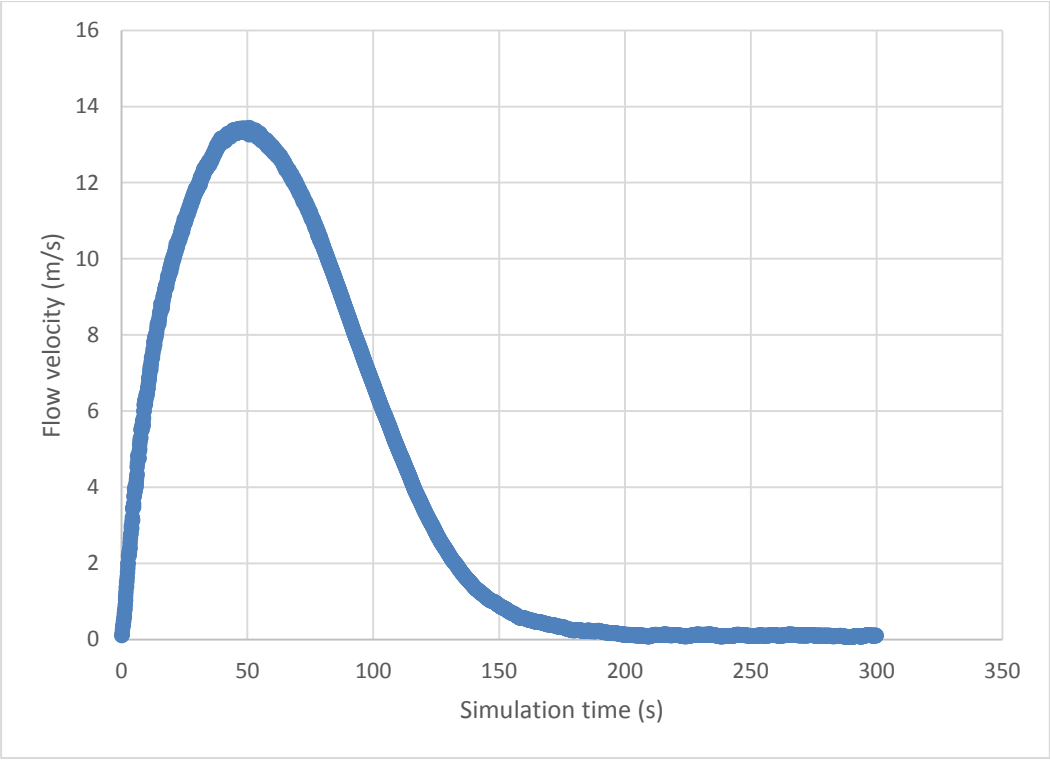

Figure 36: Analysis of flow velocity vs. simulation time.

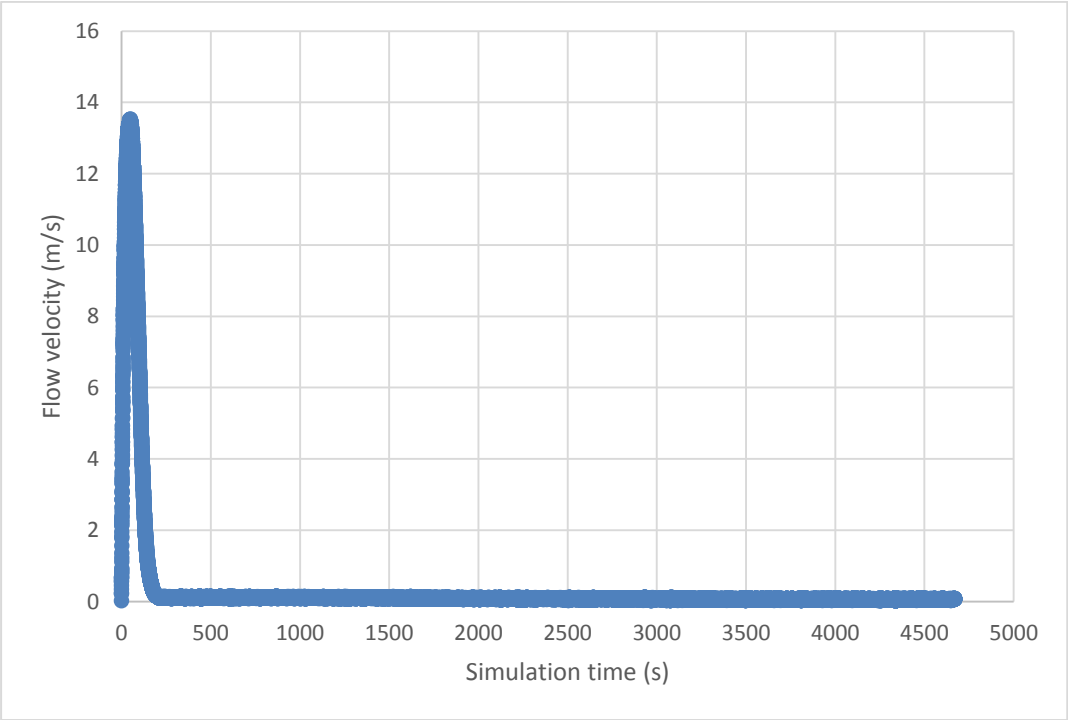

Figure 37: Analysis of flow velocity vs. simulation time.

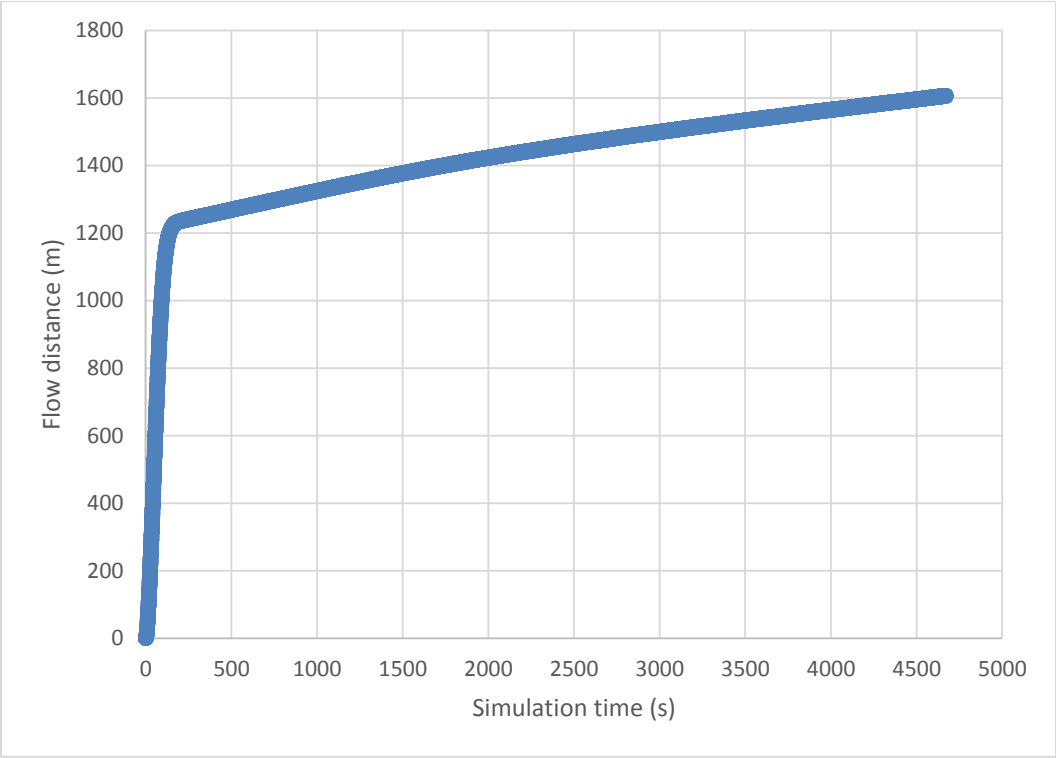

Figure 38: Analysis of flow distance vs. simulation time.

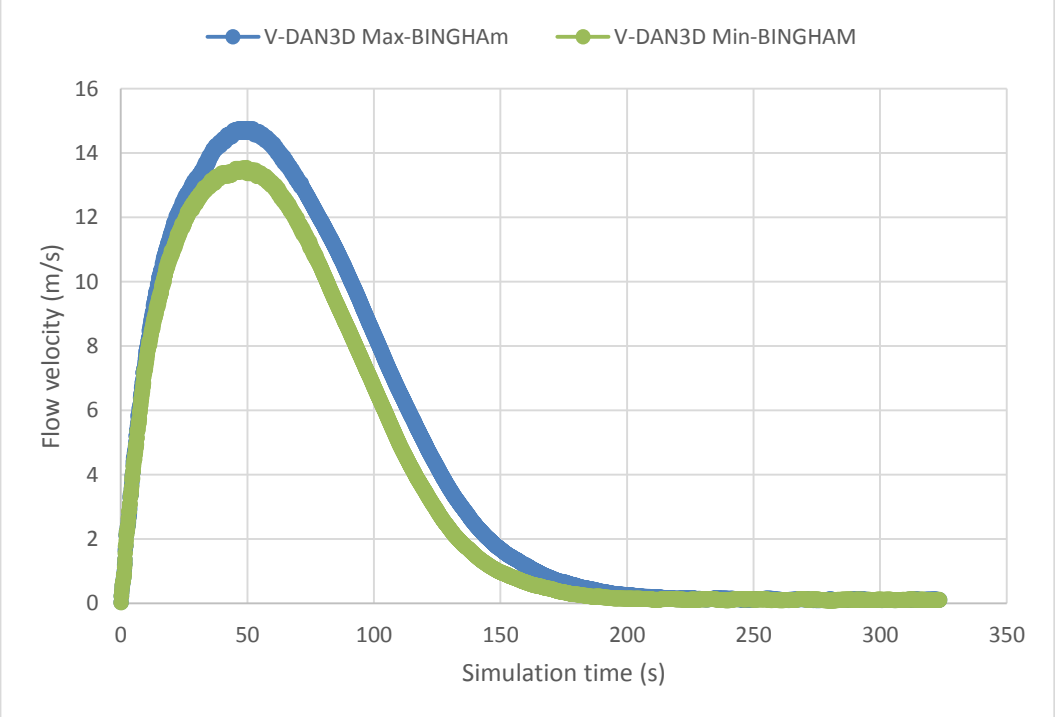

Figure 39: Comparing both volumes using Bingham rheology (flow velocity vs. time).

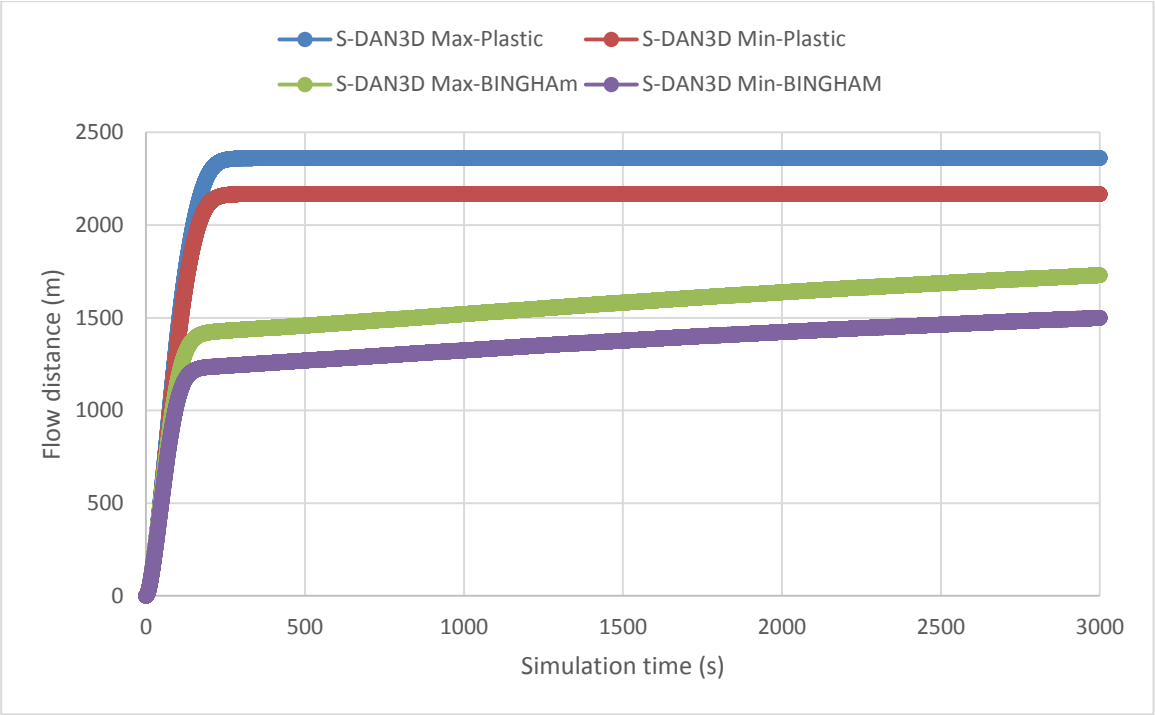

Figure 40: Comparison of both rheologies in the case of Finneidfjord landslide runout distance versus time.

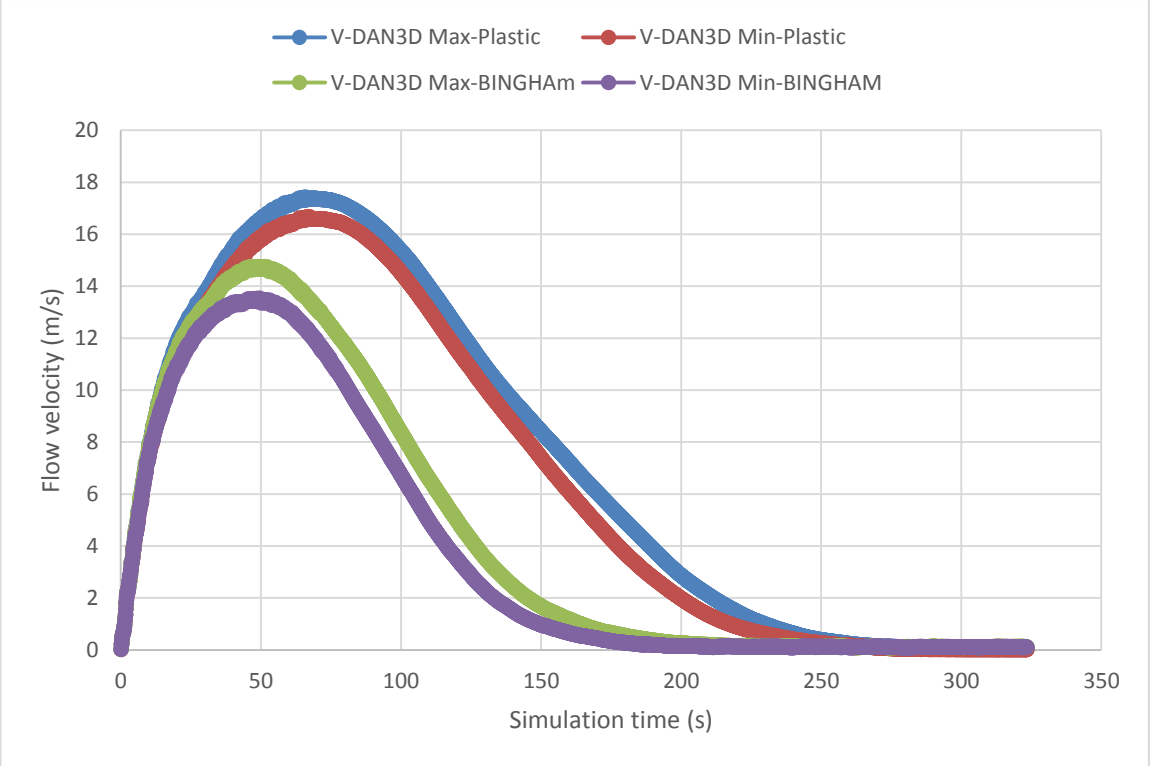

Figure 41: Comparison of both rheologies in the case of Finneidfjord landslide flow velocity versus time.

Simulation results of maximum thickness of the model were running. The results of the simulations are shown in Figure 42 and Figure 43. As it is shown in the map, the maximum thickness was the same for both cases. Because it showed the slide that passed by each grid node from the beginning of the simulation. It was also compared the thickness of the deposit using DAN3D model simulation for both rheologies. It is shown in Figure 44.

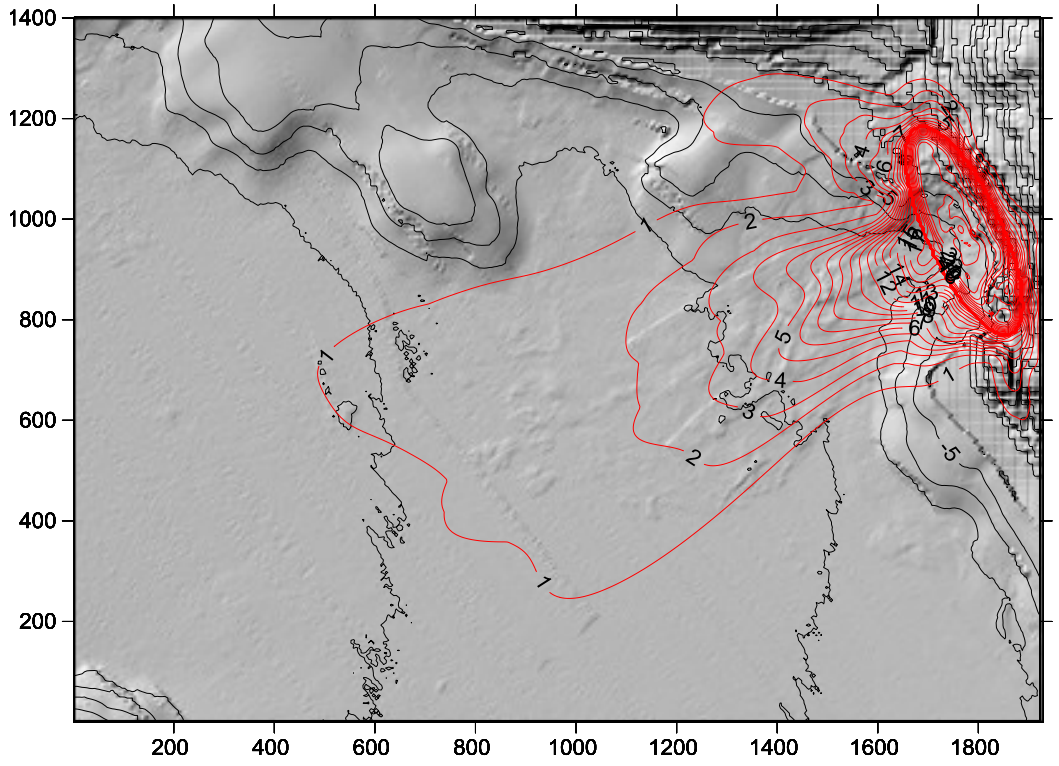

Figure 42: Maximum thickness of the deposit at simulation time of 10 seconds (maximum volume using plastic rheology).

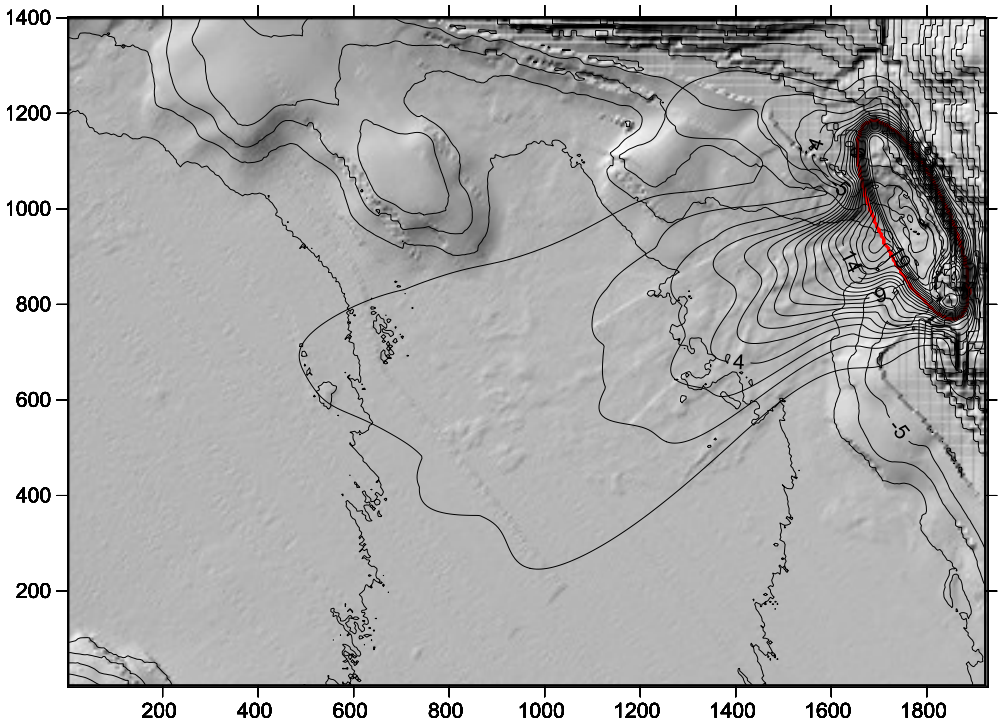

Figure 43: Maximum thickness of the deposit at simulation time of 5000 seconds (maximum volume using plastic rheology).

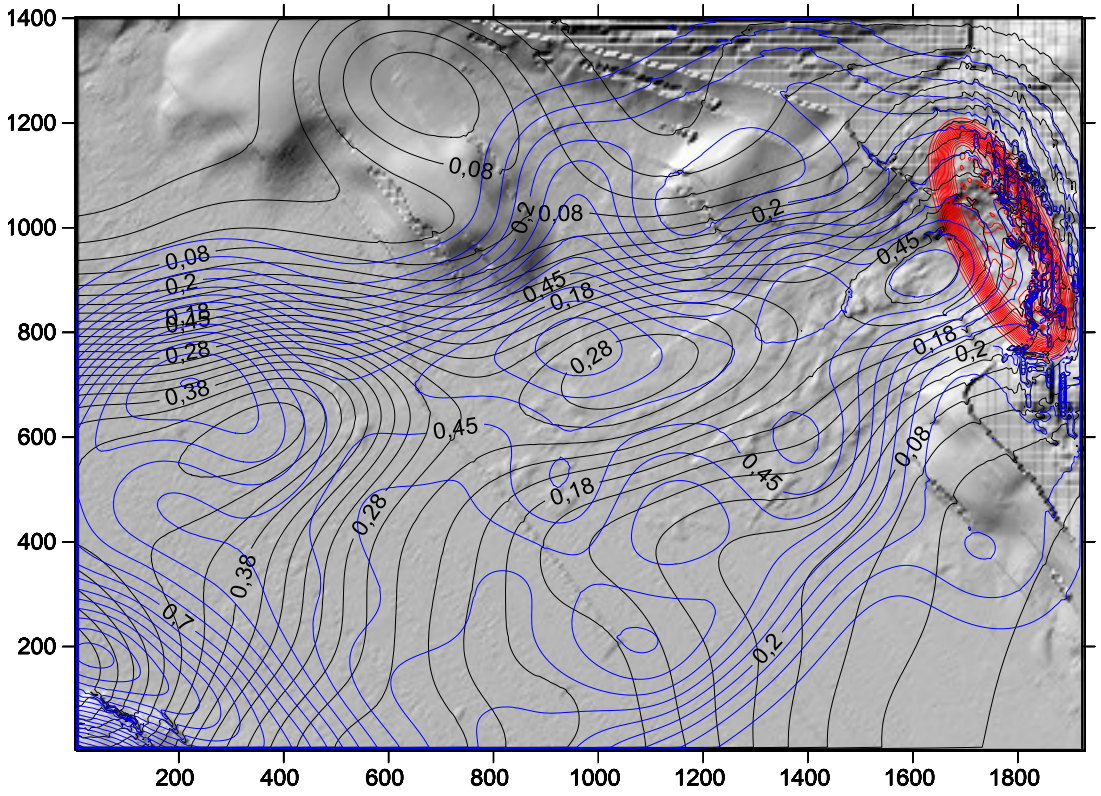

Figure 44: Plastic (black contour line) and Bingham (blue contour line) rheological simulation of flow distance and flow thickness of the slide for Finneidfjord landslide. Thicknesses of the flow are displayed in the map.

3.3.2 BING model

Finneidfjord landslide was simulated with BING model using Bingham rheology and the different running results are presented in Table 3. The geometrical requirements for BING were defined from the topography of the study area. In addition to this bed files were created using ArcGIS software that was used as input file to run BING model. Different analyses were done as shown in Figure 45, Figure 47 and Figure 49.

Table 3: BING rheological and numerical values used to run Bingham rheology for Finneidfjord landslide.

Run no.	γ_r	γ	n	ρ_q	ρ_w	No of nodes	Artificial viscosity	Runout (m)	Max. Front Velocity (m/s)
1	10.2	800	1	1880	1000	100	0.0001	1748	20.8
2	10.2	800	1	1880	1000	10	0.0001	1829	23.6
3	10.2	800	1	1880	1000	10	0.001	1660	23.8
4	10.2	800	1	1880	1000	21	0.001	1787	23.1
5	10.2	800	1	1880	1000	10	0.01	1417	21.4
6	10.2	800	1	1880	1000	60	0.001	1750	23.19

Remark: Rheological parameters are the same as in case for DAN3D model.

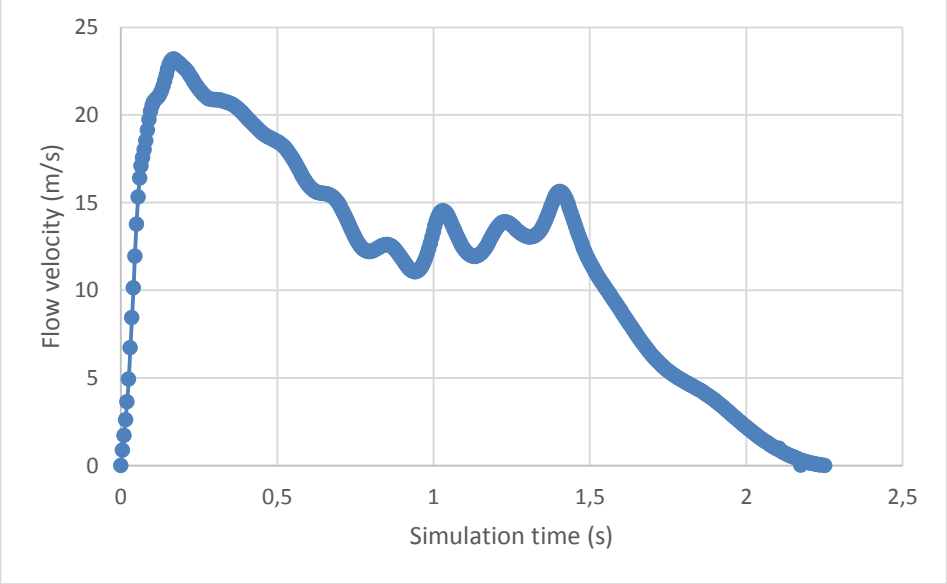

Figure 45: Analysis of flow velocity vs. time using BING model.

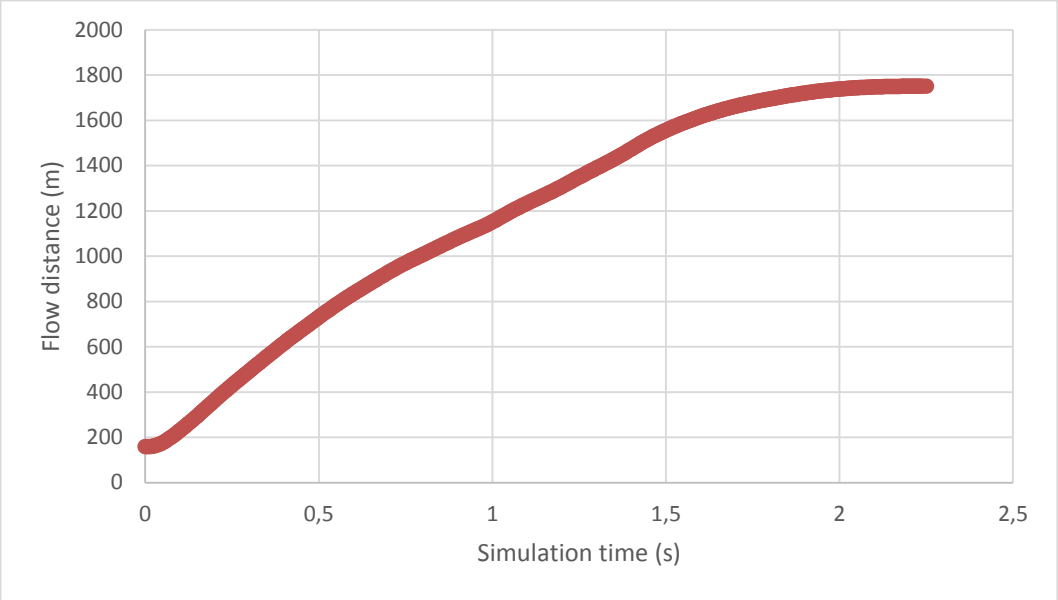

Figure 46: Analysis of runout distance vs. time using BING (Run no. 6 in Table 3).

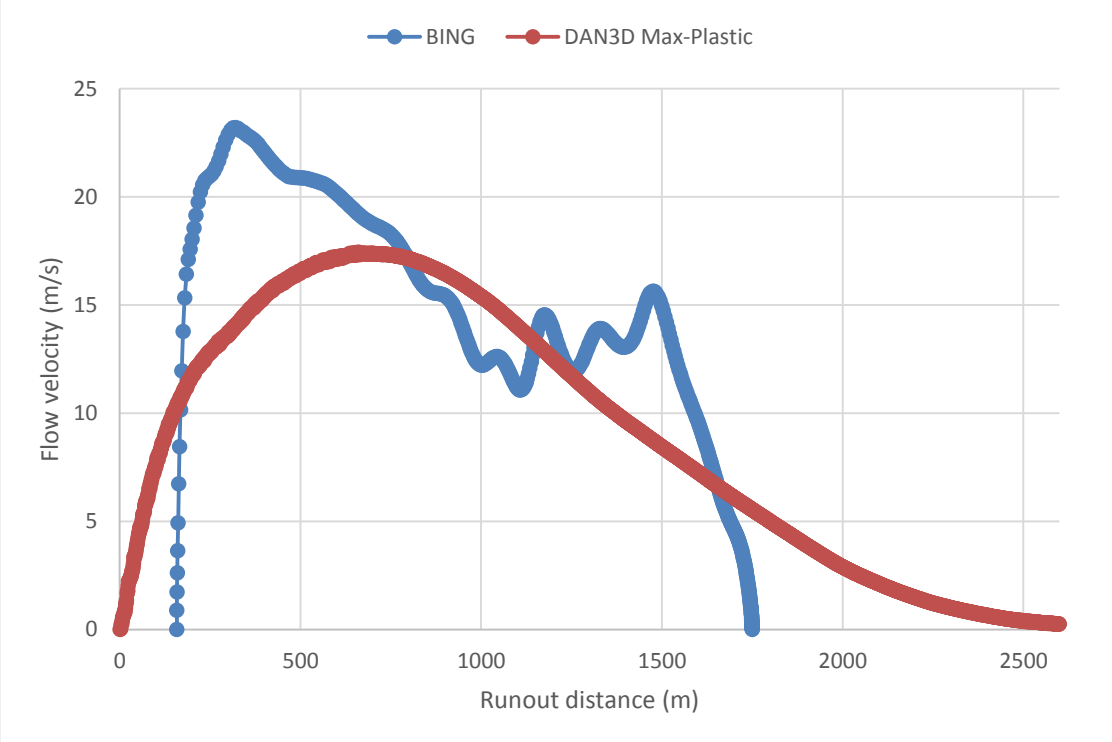

Figure 47: Analysis of flow velocity vs. runout distance using both DAN3D (plastic rheology with maximum volume) and BING.

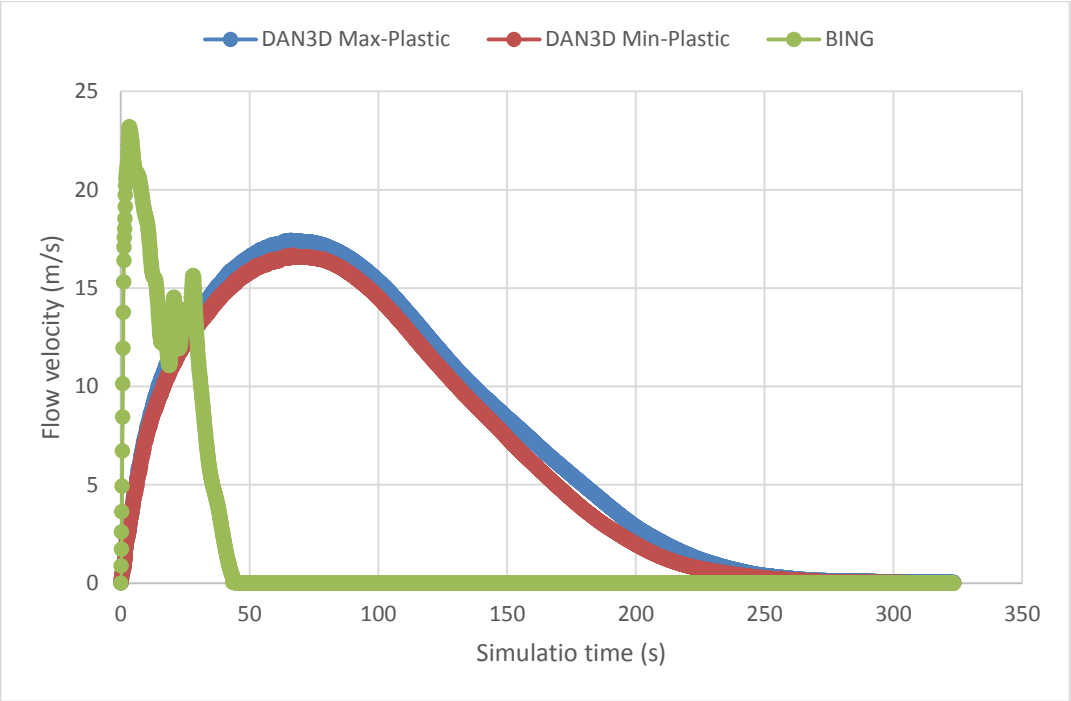

Figure 48: Comparison of flow velocity for both DAN3D (plastic) and BING model (Run no. 6 in Table 3).

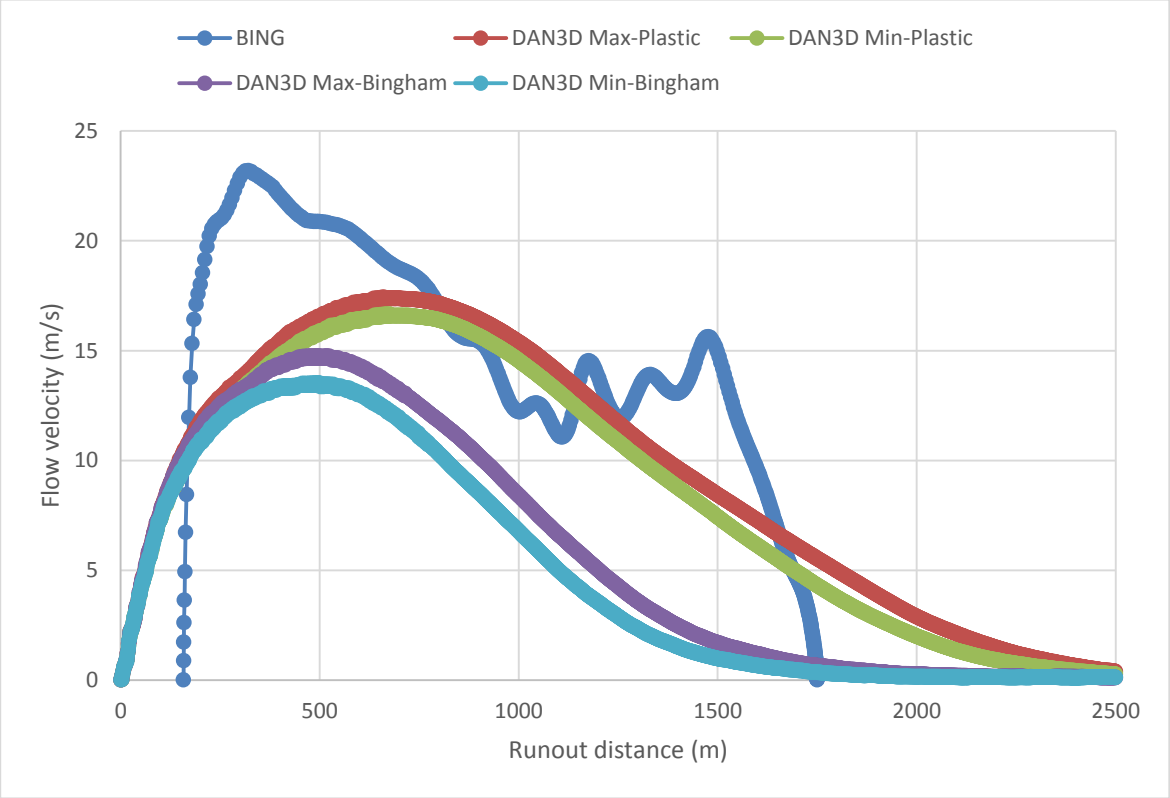

Figure 49: Comparison of both rheologies of DAN3D and BING for the Finneidfjord landslide (flow velocity vs. runout distance).

4. Discussion of simulation results of the models

Based on the result of different simulations, the following discussion and observation are presented separately for both DAN3D and BING models for each case (synthetic benchmark and Finneidfjord landslide). Detail explanations for each simulation cases are shown in section 4.1 and 4.2 respectively.

4.1 Benchmarking

Simulation of the synthetic DEM for benchmarking was done using both DAN3D and BING models. The result of this benchmarking was presented in section 3.2 above. Simulation of DAN3D model was run for different time as shown in Figure 14, Figure 15 and Figure 17. In the case of plastic rheology, both runout distance and flow velocity increase for some values and reach maximum then fall again to zero in the case of flow velocity (Figure 15) but in the case of runout distance, it become constant value as shown in Figure 14. Actually, this simulation showed the runout distance reached its maximum distance and then become to constant value. Here, the analysis showed reasonable results that have reached about the maximum runout distance 22 m and maximum flow velocity 2.8 m/s. In addition to plastic rheology, Bingham rheology was also simulated for this benchmark. However, simulation of Bingham rheology did not show similar trend as in the case of plastic rheology (Figure 16 & Figure 17). Here in this simulation, runout distance of the benchmarking was increasing infinitely which was not coming to one point as in the case of plastic rheology (Figure 16) and flow velocity has shown first rapid increasing and then falling, finally come to constant value as it is shown in Figure 17. In contrary to plastic rheology, Bingham rheology did not show how much the simulation was running (Figure 16) even though the flow velocity become constant after falling from the maximum velocity (Figure 17).

Like DAN3D model, BING model was simulated using the same rheological parameters as in the case of Finneidfjord landslide (Table 1) and some of the running results were presented in Table 2. The runout distances and peak front velocities have shown different values but the range was not a big difference values. They were almost in similar range. One of the simulations was used for further analysis (Run no. 1). The graph shown in Figure 18

drew using flow velocity vs. simulation time. This graph showed the process of moving and stopping of simulation within a limited time. Simulation time was very short (Figure 18).

Comparison between the two models was done for the benchmarking. It has shown using flow velocity versus simulation time as presented in Figure 19. As you can see in the Figure 19, the process of moving and stopping the simulation were very fast in the case of BING model. Simulation time in the case of BING model was very small when it compared with the simulation time of DAN3D model. This could be associated with the complexity of DAN3D model. In addition to this comparison was made between the flow distance and simulation time for both models as it is presented in Figure 20. Simulation with DAN3D model has longer runout distance than BING model (Figure 20). Runout distance versus flow velocity was also compared as it is shown in Figure 21, BING model simulation has higher velocity even though BING overestimates velocity of very large slides as it was mentioned in Issler et al., (2012) by De Blasio et al., 2003 and lower runout distance where as DAN3D model simulation has lower velocity and higher runout distance.

4.2 Finneidfjord landslide

Simulation of Finneidfjord landslide was done using both DAN3D and BING models by taking the rheological parameters in Table 1. The different discussion and observation are as follow:

4.2.1 Plastic rheology

The results of simulations were presented in section 3.3.1.1 using plastic rheology. First simulation was run using maximum volume of the slide. Using the output files from the simulation, flow distance and flow velocity were analyzed. Flow distance of the slide (model) increased for the simulation up to 200 seconds and then changed to constant value as shown in Figure 23. The maximum runout distance analyzed in this case was about 2300 m (Figure 23). Flow velocity of the slide increased for the first 70 seconds simulation time and reached maximum velocity, then started to decline and become constant value (zero) as displayed in Figure 24. Its maximum flow velocity was about 17 m/s. Second simulation was done taking the minimum volume of the slide using plastic rheology. The maximum runout was about 2100 m and this was happened at the simulation time of 200 seconds (Figure 27).

Its maximum velocity was about 16.5 m/s (Figure 28). When we compared both simulation runout distance to the real case reported in Issler et al., (2012), this runout distance was longer. In the real case, the runout distance ranged from 200 to 800 m for the three main stage of slides. Therefore, runout distance in this simulation travelled longer distance than the real case. This could be related to the volume considered in the simulation. In addition to this, the slide did not occurred at one stage. The energy is high in higher volume and results longer runout distance as compared to the real case. Comparison of both volumes was also prepared using flow velocity versus simulation time. They have shown similar trends but different maximum velocities. As you can see in the Figure 30, the simulation that was running with higher volume has higher maximum velocity and vice versa. Having higher volume is related to derive the slide with a maximum velocity. This is idea was mentioned by De-Blasio, (2011). Maximum velocity versus time that observed by each grid node since the beginning of the simulation in both cases are shown in Figure 25 and Figure 29. Because of the volume difference, the maximum velocity attained by the maximum and minimum volumes were about 450 m/s and 150 m/s respectively.

Based on the simulation results, it has tried to compare the deposit of the slide shown in Figure 3 and the simulation of the flow deposit for both volume of simulations, the flow contour or deposit at simulation 50 seconds (Figure 22 & Figure 26) showed similar to the real slide deposit but not other simulations. Therefore, according to this result, the simulation matched with real case in the lower time limit as shown in Figure 22 and Figure 26.

4.2.2 Bingham rheology

Bingham rheological simulations are presented in section 3.3.1.2 using the same rheological parameters like plastic rheology and dynamic viscosity of the quick clay. Similar to others, using the output files further analysis was done. In this simulation, the runout distance was increasing very fast for the first 200 simulation time and then increase slowly for the rest of simulation time of the model (Figure 38). It was still increasing slowly as the simulation was running and it cannot come to a convergent point like in the case of plastic rheology even after running the model for greater than 5000 seconds simulation time (Figure 38). Therefore it was not possible to know the runout distance. Flow velocity was also taking into consideration. As it is shown in Figure 37, flow velocity was increasing very fast for the first 49 simulation time and then reached maximum flow velocity (13.53 m/s) at the simulation

time of 49 seconds. Runout distance and flow velocity versus simulation time were also presented in Figure 32 and Figure 33. This was analyzed part of the simulation data to see clearly the graph. After the maximum flow velocity was reaching, it was declined and finally approaching to zero (Figure 37). Both simulations showed similar simulation process. Runout distance in this simulation was shorter when we compared it with the plastic rheological simulation (Figure 32 and Figure 35). This comparison was done for the first 200 seconds simulation times. As we have seen in the case of plastic rheology, Bingham rheological simulation model also showed similar slide deposit at 50 seconds simulation time (Figure 31 & Figure 34) with real slide deposit (Figure 3). When we see the other simulation cases, they have shown different deposits all over the simulation in contrary to the real case that is shown in Figure 3. In addition to these, the maximum thickness of deposit in the simulation shown in Figure 42 and Figure 43 had similar deposit in both cases, this was related to the constant volume throughout the simulation and they have shown similar to the real case deposit shown in Figure 3 except the front part of the deposit.

Assuming the same simulation time (130 seconds) and same volume slide, flow distance and thickness of the deposits were different. This difference could be because of dynamic viscosity for the case of Bingham rheology (blue contour lines) and yield stress for the plastic rheology (black contour lines). In the case of plastic rheology, the flow distance and its thickness was fast and thin in thickness (Figure 44). The second case is vice versa of the plastic rheology (Figure 44). Red contour lines in the map show the release area of the slide.

Comparison between the two models was done for Finneidfjord landslide. As you can see from Figure 47, runout distance against flow velocity was taken to see the relationship between them. Simulation with DAN3D model has longer runout distance than the BING model and maximum velocity was higher in the case of BING model than DAN3D model (Figure 47). Flow velocity versus simulation time was also considered, as it is shown in Figure 48, BING model has higher velocity and small simulation time and vice versa. In addition to this, comparison of both rheologies in DAN3D and BING was prepared as shown in Figure 49. Maximum runout distance was occurred in the simulation of DAN3D using max-Plastic and minimum runout was seen in the case of simulation BING. Runout distance using Bingham rheology in the case of DAN3D simulation, laid in between the two simulation.

5. Conclusions and recommendations for future work

5.1 Conclusions

A synthetic benchmarking and the Finneidfjord quick-clay landslide were considered as case studies for this thesis work and were simulated using the DAN3D and BING models. The models require as input the terrain models of the path and the mass at the release area, the remoulded shear strength, and the dynamic viscosity. The output files of the simulations that were of main interest for this study were analysed to calculate the runout distance and the flow velocity.

In the synthetic benchmarking simulation, the runout distance and the flow velocity showed the process of moving and stopping the simulations for the DAN3D plastic rheology. In this case, it was apparent the time when the simulation was moving and when it stooped. However, in the simulation using DAN3D Bingham rheology the runout exceeded the limits of the domain geometry. Here the model has shown inconsistency that Bingham rheology has longer runout compared to plastic rheology under the same yield strength. The benchmarking was also simulated using the BING model; the simulation time was very small when it was compared with DAN3D model. The runout and flow velocity were for both cases. The runout distance was longer in the DAN3D model simulation using plastic rheology and maximum velocity was higher for BING simulation.

The Finneidfjord landslide was simulated using both plastic and Bingham rheology in the DAN3D model for minimum and maximum volume of slides. The volumes were taken from the three stages of the Finneidfjord landslides by taking the minimum and maximum volumes from previously reported study. This case was also running using the BING model. The maximum runout distances of the simulations were about 2300 m and 2100 m for the maximum and minimum volumes respectively using plastic rheology. Velocities of the runouts were 17 and 16.5 m/s. The shape of deposit was compared and it was similar at the simulation time of 50 seconds for the two volumes.

Similarly, Finneidfjord landslide was simulated using DAN3D model (Bingham rheology) by considering the minimum and maximum volume of slide. The runout of the simulation

was compared with the plastic rheology for the first 200 seconds running time and it was found that runout distance in the case of Bingham was shorter. However, similar to the benchmark simulation runout distance exceeded the limit of the domain geometry.

In general, runout distance was the longest for case of DAN3D model in the simulation time of up to 200 seconds and the highest maximum velocity occurred in the case of BING model. The running time of the simulation using the BING model was very fast which was about less than few seconds and quick whereas the DAN3D simulation took much longer time which was about 200 seconds that considered in the analysis of runout distances and flow velocities and it was slow process model compared to the BING model.

5.2 Future work

For future work, more has to be done to characterize flow behaviour of quick-clay especially on the determination of the dynamic viscosity. Laboratory tests have to be carried out to validate the applicability of the model for failures in quick clay slides. The model is dependent on physical parameters in addition to the topography, DEM of the area that was taken in to consideration.

Volume of the release area were recorded in ranges, this may not be good to the model because the model takes one value of volume, so additional field data should allow clarifying the exact volume of slide that had occurred.

The landslide in the case of Finneidfjord was retrogressive and the model could not replicate in one simulation these multiple slides, so further investigation is needed for the model to include retrogressive slides.

References

BLANC, T., PASTOR, M., DREMPETIC, M. S. V. & HADDAD, B. 2011. Depth integrated modelling of fast landslide propagation. *European Journal of Environmental and Civil Engineering,* 15:sup1**,** 51–72.

CLAGUE, J. J. & STEAD, D. 2012. *Landslides: types, mechanisms and modeling,* Cambridge, Cambridge Univ. Press.

DE-BLASIO, F. V. 2011. *Introduction to the Physics of Landslides*.

HUNGR, O. 1995. A model for the run-out analysis of rapid flow slides, debris flows and avalanches. *Canadian Geotechnical Journal,* 32**,** 610–623.

HUNGR, O. 2010. Dynamic analysis of landslides in three dimensions. Beta 2 ed.

HUNGR, O. & MCDOUGALL, S. 2009. Two numerical models for landslide dynamics analysis. *Computers and Geosciences,* 35**,** 978–992.

IMRAN, J., HARFF, P. & PARKER, G. 2001a. A numerical model of submarine debris flow with graphical user interface. *Computers and Geosciences,* 274**,** 717–729.

IMRAN, J., PARKER, G., LOCAT, J. & LEE, H. 2001b. 1D Numerical modelL of muddy subaqeous andsubaerial debris flows. *Journal of Hydraulic Engineering,* 127**,** 959–968.

ISSLER, D., CEPEDA, J. M., LUNA, B. Q. & VENDITTI, V. 2012. Back-analyses of run-out for Norwegian quickclay landslides. Norwegian Geotechnical Institute (NGI).

JIANG, L. & LEBLOND, P. 1993. Numerical modeling of an underwater Bingham plastic mudslide and the waves which it generates. *Journal of geophysical research,* 98**,** 10303–10317.

L'HEUREUX, J.-S. 2012. Characterization of historical quick clay landslides and input parameters for Q-Bing. Norwegian Geotechnical Institute, Oslo, Norway

L'HEUREUX, J.-S., EILERTSEN, R. S., GLIMSDAL, S., ISSLER, D., SOLBERG, I.-L. & HARBITZ, C. B. 2012. Submarine mass movements and their consequeces. *In:* YAMADA, Y., KAWAMURA, K., LKEHARA, K., OGAWA, Y., URGELES, R., MOSHER, D., CHAYTOR, J. & STRASSER, M. (eds.) *5th International symposium.* Springer.

LONGVA, O., JANBU, N., BLIKRA, L. H. & BØE, R. 2003. The 1996 Finneidfjord slide; Seafloor failure and slide dynamics. *Submarine mass movements and their consequences.* Netherlands: Springer.

LUNA, B. Q. 2008. Benchmarking of debris flow runout distance; simulation of Frank slide and Shum Wan Road landslide, International center for Geohazards Report 2008-7-1.

LUNA, B. Q. 2012. *Dynamic numerical run-out modeling for quantitative landslide risk assessment.* PhD Dissertation Univerity of Twente.

LØKEN, T. 1983. Kvikkleire og skredfare – hvor og hvorfor? *Forskningsnytt fra Norges almenvitenskapelige forskningsråd,* 28 (3)**,** 7 – 12.

MCDOUGALL, S. 2006. *A new continuum dynamic model for the analysis of extremely rapid landslide motion across complex 3D terrain.* . PhD thesis, University of British Columbia.

MCDOUGALL, S. & HUNGR, O. 2005. Dynamic modeling of entrainment in rapid landslides. *Canadian Geotechnical Journal,* 42**,** 1437–1448.

MONAGHAN 1992. Smootheed Particle Hydrodynamics. *Annual Review of Astronomy and Astrophysics* 30**,** 543-574.

NATTERØY, A. 2011. Skredkatalog om kvikkleire. *Presentasjon av det førebels resultatet i katalogen og utgreiing om typiske kjennetegn ved kvikkleireskred. Prosjektoppgave.* Institutt for geologi og bergteknikk, NTNU.
NGF 1974. Retningslinjer for presentasjon av geotekniske undersøkelser. Norsk Geotekniske Forening, Oslo, Norway.
NIGUSSIE, D. G. 2013. *Numerical modelling of run-out of sensitive clay slide debris.* MSc Thesis, Norwegian University of Science and Technology.
NVE 2009. Retningsliner for planlegging og utbygging i fareområder langs vassdrag. Norwegian Water and Energy Directorate (NVE), Oslo, Norway.
PASTOR, M., HADDAD, B., SORBINO, G., CUOMO, S. & DREMPETIC, V. 2009. A depth-integrated, coupled SPH model for flow-like landslides and related phenomena. *International journal for numerical and analytical methods in geomechanics,* 33**,** 143–172.
PASTOR, M. & LUNA, B. Q. 2012. Safeland. *In:* CROSTA, G. (ed.) *Living with landslide risk in Europe: Assessment, effects of global change, and risk management strategies.*
PIRULLI, M. 2005. *Numerical modelling of landslide runout.* PhD thesis, Politecnico Di Torino.
WOLDESELASSIE, B. H. 2012. *The effect of blasting in layered soils, example from Finneidfjord, Norway* [Online]. MSc. Thesis, NTNU, Norway: http://www.diva-ortal.org/smash/get/diva2:565987/FULLTEXT01.pdf. [Accessed on 09 December 2014].

Appendix 1: Preparation of input files for DAN3D

The back analysis done for Finneidfjord slide preparation needs input data that are necessary for the simulation of the model (DAN3D). ArcGIS 10.2.2 and Surfer 11 (Golden software) were used to prepare the input files to run the simulations. Some of the steps used to prepare the input files:

The following steps were done to prepare the path topography file of Finneidfjord slide:

1. In order to avoid overlapping between the Fjord and the land, it has been created a TIN (Triangular irregular network) between bathymetry of the fjord and the land (contours).
2. Converting the TIN to raster dataset (DEM)
3. Mosaicking the raster dataset (step 2) and existing Bathymetry ((Bathy_Sorfifjord_utm33.ers) – the name is taken from the data base of the NGI) of Finneidfjord
4. Clipping or extracting the raster dataset (step 3) to the study area
5. After clipping, it has been tried to check the quality of the raster data set by creating the slope, flow direction and flow accumulation.
6. Convert the raster dataset (step 4) to ASCII files.
7. Open surfer and open the ASCII file with common file then it has to save in the surfer 6 text grid (*.grd) extension. This file extension is compatible to DAN3D.
8. Then take these files (step 7) as input to DAN3D model.

The following steps were done to prepare the source topography file of Finneidfjord slide:

1. Multiply the path topography dataset (step 4 above) by zero.
2. Calculate the thickness of source topography from the extracted release area by taking the volume and area of release area. However, for this study it has considered from the NGI report volume and area of the elliptical polygon from the analysis.
3. Create raster dataset using step 1 (zero raster dataset) and thickness of the release area (Zero raster + thickness of release area).
4. Clip or extract the raster dataset by using the elliptical polygon.
5. The last step is mosaicking the zero raster and clipped raster dataset (step 1 and step 4) to make the same size as the path topography.

Appendix 2: Overview of the types of landslide that occurred in the Norwegian quick clay

No	Location	Date	Type of landslide	Volume (m^3)	$W_{avg.}$	L (m)	D (m)	H_D (m)	Reference
1	Bakklandet	10.11.1634	Flow	500 000	130	75			Bjerrum & Kjærnsli (1957)
2	Bekkelaget	07.10.1953	Flake	100 000	160	165	20		Eide & Bjerrum (1955)
3	Brå	01.05.1928	Flake	500 000	500	200	400	20?	Holmsen (1929)
4	Byneset	01.01.2012	Flow	350 000	100	400	900	3	NVE files, Thakur (2012)
5	Båstad	05.12.1974	Spread	1 500 000	450	325	700	3	Gregersen & Løken (1979)
6	Drammen	06.01.1955	Spread	4 000	50	45			Bjerrum & Kjærnsli (1957)
7	Døla	19.06.2011	Spread	30 000	50	65	30		NGI (2011)
8	Hyggen	23.01.1978	Flow	500 000	100	40	450		Karlsrud (1979), Hansen et al. (2011)
9	Duedalen	18.07.1625	Flow	500 000	195	380			L'Heureux (2012)
10	Fallet, Rissa	1997	Flow	200 000	130	150	670		L'Heureux et al. (2011)
11	Finneidfjord	20.06.1996	Flow	1 000 000	300	150	1000	1.4	Longva et al. (2003)
12	Fredrikstad	17.08.1980	Spread	10 000	25	50	30		Karlsrud (1983)
13	Furre	14.04.1959	Flake/Spread	3 000 000	720	400	0-90		Kenney (1967)
14	Gretnes	17.04.1925	Flow	400 000	220	210			Holmsen (1929)
15	Gullaug 1	29.11.1974	Flow	100 000	190	40	325		Karlsrud (1979), Hansen et al. (2011),
16	Gullaug 2	Pre-historical	Flow	100 000	380	500			L'Heureux (2012)
17	Heimstad	Pre-historical	Flow	900 000	220	370			L'Heureux (2012)
18	Hekseberg	20.03.1967	Flake	200 000	150	160	300		Drury (1968)
19	Kattmarka	13.03.2009	Spread and flow	600 000	80	300			Nordal et al. (2009)
20	Kokstad	21.10.1924	Spread and flow	400 000	180	180	600		Holmsen (1929)
21	Lade	11.04.1944	Spread	50 000	210	25	100		Holmsen & Holmsen (1946)
22	Langørjan	Pre-historical	?	11 000 000	1000	500			L'Heureux (2012)
23	Leirfossen	Pre-historical	?	75 000 000	1200	3500			L'Heureux (2012)
24	Lodalen, Oslo	06.10.1954	Spread	10 000	50	40			Sevaldson (1956)
25	Lund	Pre-historical	Flow	4 600 000	500	1050			L'Heureux (2012)
26	Lyngseidet	03.09.2010	Flow	220 000	120	160	420		L'Heureux (2012)
27	Olderdalen	Pre-historical	Flow	25 000 000	450	1600			L'Heureux (2012)
28	Othilienborg	Pre-historical	Flow	70 000 000	1000	1700	11000		L'Heureux et al. (2009)
29	Rissa (initial)	29.04.1978	Flow	150 000	80	450	620		L'Heureux et al. 2012
30	Rissa (main)	29.04.1978	Flake and Flow	5 000 000	400	1400	1200	6	Gregersen (1981), L'Heureux et al. 2012
31	Rørdal	Pre-historical	?	3 300 000	270	890			L'Heureux (2012)
32	Selnes	18.04.1965	Spread and flow	140 000	166	215	400	2	Kenney (1967)
33	Skjelstadmarka	14.08.1962	Flow	2 000 000	200	600	2240		Trak & Lacasse (1996)
34	Sjetnemarka	Pre-historical	Flow	30 000 000	1100	1050			L'Heureux (2012)
35	Stavset	Pre-historical	Flow	800 000	200	125			L'Heureux (2012)
36	Tiller	07.03.1816	Flow	550 000	610	350			L'Heureux (2012)
37	Ullensaker	23.12.1953	Flow	200 000	180	195	1500	4	Bjerrum (1955)
38	Verdal	19.05.1893	Flow	65 000 000	1000	2000	9000		Trak & Lacasse (1996)
39	Vibstad	22.02.1959	Spread	1 400 000	325	250	250		Bjerrum (1955)

Adapted from (L'Heureux, 2012).

Appendix 3: Geotechnical parameters of the landslides presented in appendix 2.

No	Location	γ (kN/m3)	s_u (kPa)	Max S_t	s_{ur} (kPa)	I_P	I_L
1	Bakklandet	18.9	10–19	210	0.07	7	1.8
2	Bekkelaget	18.9	10	80	0.13	9	2.4
3	Brå	19.0	18	75	0.24	5.5	2
4	Byneset	18.3	10–25	113	0.20	5	4.2
5	Båstad	19.3	30–40	100	0.65	6	1.6
6	Drammen	19.1	20	4	2.00	14.2	0.8
7	Døla	20.0	12	40	0.3	7.7	1.8
8	Hyggen	19.0	10	20	2.00	-	0.5
9	Duedalen	18.9	10–19	210	0.07	4	4.0
10	Fallet, Rissa	18.4	15–20	12	0.8	5	1.2
11	Finneidfjord	18.8	7–10	100	0.08	6.00	2.5
12	Fredrikstad	19.0	15	20	0.9	20	1
13	Furre	19.0	35–45	30	0.67	10	2.3
15	Gullaug 1	19.0	12	4	3.00	10	1
18	Hekseberg	19.0	20–30	150	0.17	7	3.2
19	Kattmarka	19.0	15	60	0.25	6	3
21	Lade	19.2	20–30	16	1.56	10	1.00
24	Lodalen, Oslo	19.1	45	3	15	18	0.72
26	Lyngseidet	19.2	5	52	0.15	7	2.4
27	Olderdalen	20.0	20–30	70	0.43	4	3
28	Othilienborg	19.3	10–25	83	0.30	4	4.2
29	Rissa 1	18.6	10–20	100	0.24	10	2.3
30	Rissa 2	18.6	10–20	100	0.24	5	2.3
32	Selnes	18.6	15–20	100	0.17	6	1.9
33	Sjetnemarka	20.0	23	86	0.27	4.5	2.2
34	Skjelstadmarka	19.3	40	48	0.83	6	1.6
36	Tiller	18.7	20–40	150	0.20	4	2.0
37	Ullensaker	18.6	10–25	42	0.43	7	1.2
38	Verdal	19.3	10–200	40	0.20	4	2.5
39	Vibstad	18.3	30–70	40	1.25	7	1.3

Adapted from (L'Heureux, 2012) and (Natterøy, 2011)